Journal of Building Engineering 92 (2024) 109676

Contents lists available at ScienceDirect

Journal of Building Engineering

journal homepage: www.elsevier.com/locate/jobe

Practical equations for constitutive model of design-oriented FRP-confined concrete rectangular members

Mehmet Palanci *, Ilker Subasi

Department of Civil Engineering, Istanbul Arel University, 34537, Istanbul, Turkey

ARTICLE INFO

Keywords:
Moment-curvature relation
FRP-Confined concrete
Ultimate axial stress and strain
Prediction equation

ABSTRACT

The strengthening with Fiber Reinforced Polymer (FRP) offers one of effective solution to increase strength, axial load and deformation capacity of reinforced concrete (RC) members. However, the use of FRP-confined models can diverge in reflecting FRP confinement behavior, and they require significant computational effort and time. Moreover, the use of these models and their impact on member responses is not studied. To address this, several design-oriented FRP-confined concrete models were utilized and compared by using axial load-moment interaction diagrams and the moment-curvature relationship. Comparisons revealed that compressive strength of FRP-confined members could increase to 2.5 times while axial strain capacity could increase 4.0 times compared to unconfined ones depending on FRP-confined model. Based on the statistical analysis of numerous analytical sections covering broad-range properties of FRP material, practical equations were developed for predicting compressive strength and strain at ultimate for the design and analysis of FRP-confined RC sections. The proposed equations were then subjected to a comparison with analytical and various experimental studies, and their impact on the moment-curvature responses was investigated. Results indicated that proposed equations were in a good agreement with analytical models by the correlation coefficient higher than 0.97. The mean residuals between proposed equations and experimental results were also found around the 10 %, showed that proposed model could capture the stress-strain behavior of FRP-confined concrete. Moment-curvature response produced by proposed model and existing FRP-confined models were also found comparable with experimental results.

1. Introduction

Seismic performance of reinforced concrete (RC) structures after major earthquakes was found insufficient by site investigations owing to inadequate strength, reinforcement detailing and poor quality of workmanship [1–5]. These inadequacies caused weaknesses and reduced strength and deformation capacity of building elements and hence lateral load resistance of structure, resulted in damage and collapse of structures. Analytical studies have also shown the increasing probability of collapse and damage mechanism for these type of structures [6–8]. To increase seismic capacity of these structures, strengthening is needed and both strength and deformation capacity of structural elements can be enhanced by lateral confinement [9].

Many alternatives are available for strengthening in both structural and member level. Jacketing technique is widely used, and it may be the less destructive and environmental among the others if member capacity needs to be improved. Jacketing can be made with reinforced concrete, steel plates or with Fiber Reinforced Polymer (FRP) materials [10]. FRP materials is mostly preferred because it is

* Corresponding author.
E-mail addresses: mehmetpalanci@arel.edu.tr (M. Palanci), ilkersubasi@arel.edu.tr (I. Subasi).

https://doi.org/10.1016/j.jobe.2024.109676
Received 9 March 2024; Received in revised form 6 May 2024; Accepted 20 May 2024
Available online 21 May 2024
2352-7102/© 2024 Elsevier Ltd. All rights are reserved, including those for text and data mining, AI training, and similar technologies.

light, simple to apply, it does not need special equipment, it can protect the members from chemical effects and corrosion, provides high strength for material, increases the axial load carrying capacity and lateral deformation capacity of the columns [11]. Because of many advantages given above, FRP-confinement is studied in this study. Mechanical characteristics of FRP-confined concrete under compression was investigated in-depth, and various models were developed to predict the characteristics of concrete members especially for columns confined with FRP. In the literature, both design- and analysis-oriented models haven been developed for the approximation of FRP-confined concrete behavior [11–22].

Analysis-oriented models widely recognized for their versatility in predicting the complete stress-strain curve. These models are crucial in studying the behavior of materials under various loading conditions, particularly in analyzing the deformation and failure mechanisms. Analysis-oriented models have become an essential tool in engineering and materials science research since these models approximate the complete FRP-confined concrete behavior. However, utilization of such models is often associated with a considerable investment of time due to the substantial computational efforts required. On the other hand, design-oriented models typically developed by analyzing experimental results and utilizing regression analyses. Ozbakkaloglu et al. [9] evaluated the existing predictive models and they stated that Lam and Teng [20] model effectively predicted the ultimate strength and strain out of the 68 FRP-confined models assessed. These models are considered to be design-oriented concrete models, but the limited experimental database presents a significant challenge for FRP-confined models. Studies that utilize hoop strain at FRP rupture ($\varepsilon_{h,rup}$) instead of the ultimate rupture strain of the FRP material (ε_{fu}) have yielded more promising results and the efficiency factor (k_ε) was used to bridge the gap between the ultimate (ε_{fu}) and ($\varepsilon_{h,rup}$). However, the predictions of the ultimate compressive strain of FRP-confined concrete (ε_{cu}) in the examined models have shown a larger error than the predictions of the ultimate strength of FRP-confined concrete (f'_{cu}). This error can be attributed to the varying ultimate breaking strength (ε_{fu}) of the FRP material based on its composition [9]. According to study of Lin [23], design-oriented models are more accurate in predicting results than analysis-oriented ones among the existing FRP-confined models. It was found that these models are less successful in predicting the response of FRP-confined concrete in rectangular cross-section columns compared to square columns. Moreover, Lin observed that these models are more successful in predicting the maximum axial strength of FRP-confined concrete samples that exhibit a hardening stress-strain relationship than those that display softening behavior.

Efforts have been made to develop data-driven models to determine the complete stress-strain behavior of FRP-confined models and to characterize both yield and ultimate strength and strain [24–30]. The proposed models mostly utilized the artificial neural networks (ANNs), which heavily influenced by the quality of the database and the complex and unknown parameters of the method. In addition, these models may neglect the essential input parameters that significantly influence the behavior of FRP-confined concrete [30].

The existing literature is lacking in-depth discussion about the impact of various models on the moment-curvature relationship and interaction diagram of sections when the section properties and concrete compressive strength change. To address this gap, this study utilized several well-known design-oriented concrete models to explore the moment-curvature relationship and its influence on the interaction diagram. Based on the literature studies mentioned above and the recent ACI-440 code [31], wide range FRP materials was investigated and ultimate tensile strength of FRP material was found mainly ranged between 700 and 3600 MPa. Considering the dispearancy of this parameter, wide range FRP materials was utilized, and numerous analytical FRP-confined RC sections generated using broad range of these values in this study. Accordingly, the one of the innovations of this study can be considered as the proposed model was designated to cover different type of FRP materials. Through statistical analysis, the FRP-confined strength, strain, and curvature capacities at ultimate were evaluated and practical equations to predict compressive strength and strain at ultimate for the design and analysis of FRP-confined model was developed. It should be noted that no study was found which explicitly presents the relationship between input parameters and both stress and strain capacity of FRP-confined concrete with practical mathematical expressions providing a more efficient and time-effective alternative to the traditionally complex and computationally intensive models. The other utmost advantage of the developed explicit mathematical model can be considered as a reference for new generation data-driven methods which will help to reduce the dependency of results to the input data. Finally, innovative approach was followed to evaluate the efficiency of the proposed model and the comparisons were extended for existing and proposed model in terms of moment-curvature response and moment-axial load interaction of FRP-confined models in addition to comparison of stress-strain relation.

2. Description of FRP models and method of analysis

The common FRP material types are carbon, glass, aramid and basalt. Due its high tensile strength, carbon FRP (CFRP) material is widely applied in construction applications [32]. Accordingly, moment-curvature and axial load-moment relationship of RC rectangular members were first determined using CFRP material. To represent stress-strain relationship of CFRP material, some well-known design-oriented models are used [15,17,19,22]. In addition to FRP models, RC members were modeled with Mander concrete model [33]. By this way, effect of FRP models is compared developed CFRP models and efficiency of models were introduced. For this purpose, numerous RC members were produced [34] and moment-curvature and axial load-moment (N-M) relationships were obtained. In further sub-sections, brief information about the adopted FRP models and behavior of concrete and reinforcement are provided.

2.1. Youssef model

In experimental studies of this model (referred as Youssef), total of 87 experiments including circular, square and rectangular short columns were used and confined by carbon/epoxy and E-glass/epoxy materials. In the study, parameters such as section geometry, FRP

properties, ultimate strength of materials affecting the stress-strain relationship were statistically analyzed and equations for FRP model were developed as seen in Fig. 1 [15]. It can be seen from the figure that FRP jacketing becomes active beyond the point B (f_t, ε_t). Initial increments of the stress-strain curve of FRP concrete between points A and B was modeled Hognestad parabola [35]. Later, points B and C is linearly connected by using the ultimate stress and strain values $(\varepsilon_{cu}, f'_{cu})$.

In the figure, f_t and ε_t is calculated by Eqs. (1) and (2). In these equations, notations of ρ_j, E_j, f_{ju} and f'_c are volumetric ratio, tensile modulus and strength of FRP jacket, and compressive strength of unconfined concrete, respectively. ε_{jt} can be taken equal to peak strain value of unconfined concrete which is 0.002.

$$f_t = \left(1.0 + 1.1350\left(\frac{\rho_j E_j \varepsilon_{jt}}{f'_c}\right)^{5/4}\right) f'_c \tag{1}$$

$$\varepsilon_t = 0.002 + 0.0775\left(\frac{\rho_j E_j \varepsilon_{jt}}{f'_c}\right)^{6/7}\left(\frac{f_{ju}}{f'_c}\right)^{1/2} \tag{2}$$

Ultimate strength (f'_{cu}) and strain (ε_{cu}) of FRP is calculated by Eqs. (3) and (4). In the equation, f'_{lu} is the effective lateral confining pressure at the rupture.

$$f'_{cu} = \left(0.5 + 1.225\left(\frac{f'_{lu}}{f'_c}\right)^{3/5}\right) f'_c \tag{3}$$

$$\varepsilon_{cu} = 0.004325 + 0.2625\left(\frac{f'_{lu}}{f'_c}\right)\left(\frac{f_{ju}}{f'_c}\right)^{1/2} \tag{4}$$

2.2. Pantelides model

This numerical model (referred as Pantelides) was proposed using different cross-section geometries to determine stress-strain relationship of FRP-confined concrete columns [17]. Formulation of numerical model is based on the four-parameter equation proposed by Richard and Abbot [36]. Proposed stress-strain relation model could be used for hardening or softening behavior as depicted in Fig. 2 depending on the column section property and effective confining ratio f'_{lu}/f'_c. If f'_{lu}/f'_c is higher than 0.2 then hardening behavior is preceded and vice versa. A polynomial constant (n) was used for the smooth transition between the two branches of stress-strain relationship.

f_o is calculated by using Eq. (5) for the first branch of hardening behavior. In the equation, E_o is modulus elasticity of FRP-confined concrete, β represents the rigidity constraint for FRP jacketing and ε_o is equal to 0.004. Ultimate compressive strength f'_{cc} and strain ε'_{cc} for hardening behavior is also calculated by Eqs. (6) and (7). In Eq. (7), k_ε is efficiency factor and ε_{fu} is ultimate tensile strain of FRP material.

$$f_o = \frac{E_o \varepsilon_o}{1 + \beta \varepsilon_o} \tag{5}$$

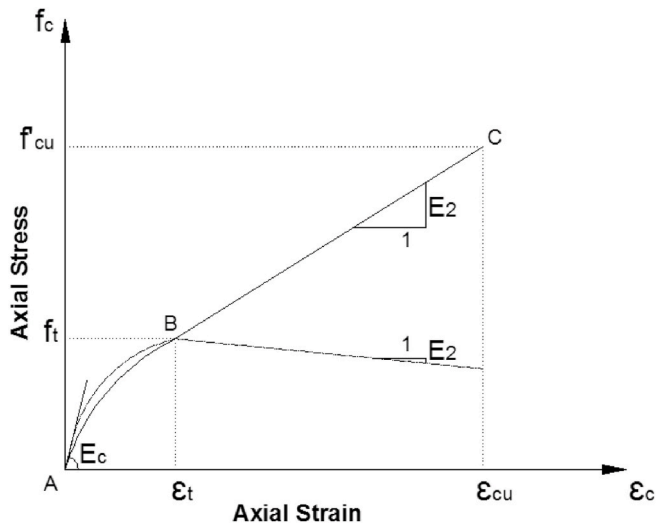

Fig. 1. Stress-strain relationship developed by Youssef et al. (2007).

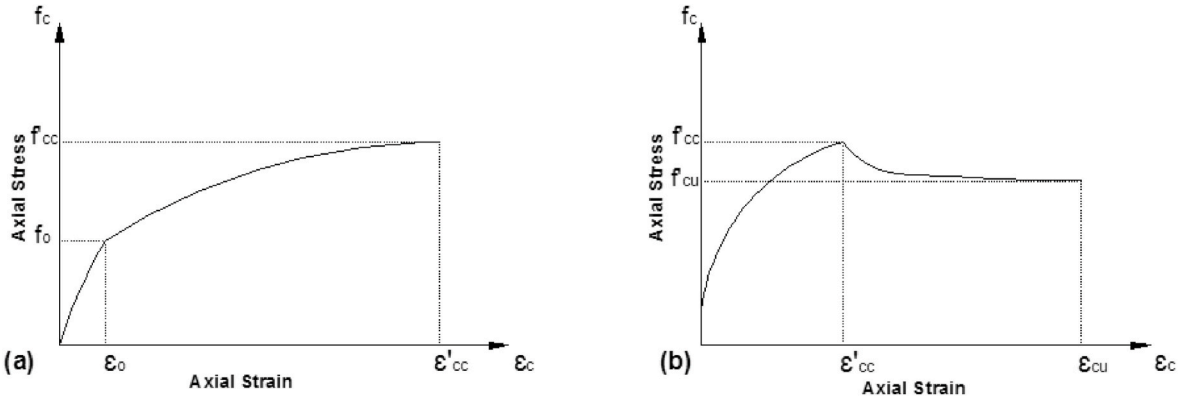

Fig. 2. Stress-strain relations a) Hardening b) softening behavior for Pantelides et al. (2004).

$$f'_{cc} = \left(-4.332 + 4.721\sqrt{1 + 4.193\frac{f'_{lu}}{f'_c}} - 2\frac{f'_{lu}}{f'_c} \right) f'_c \tag{6}$$

$$\varepsilon'_{cc} = \frac{f'_{cc}\left(1 + 2\,\beta k_\varepsilon \varepsilon_{fu}\right)}{E_o} \tag{7}$$

For softening behavior, ε'_{cc} is assumed 0.004 as given in hardening behavior. Maximum stress (f'_{cc}) at this level should be always higher than unconfined concrete strength and calculated by Eq. (6). Ultimate stress of FRP-confined section at the ultimate strain level is calculated via Eq. (8) and ultimate strain is determined by Eq. (9).

$$f'_{cu} = \left(0.0768\, ln\frac{f'_{lu}}{f'_c} + 1.122\right) f'_{cc} \tag{8}$$

$$\varepsilon_{cu} = \frac{f'_{cu}\left(1 + 2\,\beta k_\varepsilon \varepsilon_{fu}\right)}{E_o} \tag{9}$$

2.3. Lam and Teng model

Stress-strain relation equation of Lam and Teng [19,20] also adopted modified version of Richard and Abbott [36] equation and comparisons of analytical model with numerous experimental results in the literature [19,20] showed good agreement. Stress-strain relationship of Lam and Teng model is drawn with unconfined concrete model in Fig. 3. Polynomial constant (n) was used for transition of two branches for this model too. Strain reduction factor (k_ε) was considered and suggested as 0.586 for carbon FRP material in this model.

Intersection point between the two branches (ε_t) is calculated by Eq. (10). In the equation, f_o is accepted as unconfined concrete stress (f'_c) and it is the determined by the extension of second branch (linear line) slope (E_2). E_c is the elastic modulus of the unconfined concrete.

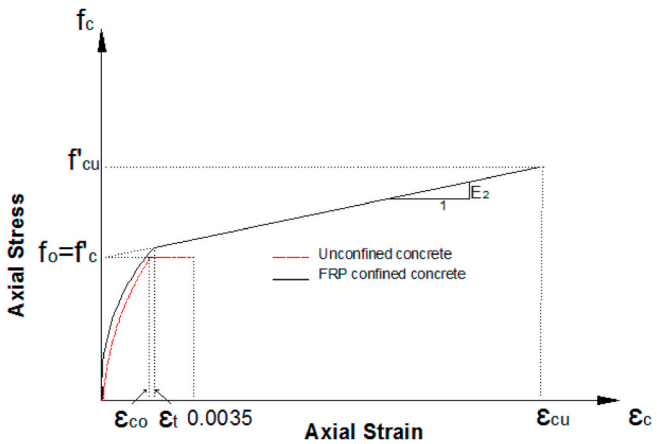

Fig. 3. Stress-strain relationship of Lam and Teng [19].

$$\varepsilon_t = \frac{2f_o}{(E_c - E_2)} \tag{10}$$

Ultimate stress of FRP-confined section (f'_{cu}) can be computed by Eq. (11). f'_{lu}/f'_c represents the nominal confinement ratio.

$$f'_{cu} = \left(1 + 3.3\frac{f'_{lu}}{f'_c}\right) f'_c \tag{11}$$

Ultimate axial strain of FRP (ε_{cu}) is obtained by Eq. (12). In the equation, $\varepsilon_{h,rup}$ notated as hoop strain of FRP at rupture. ε_{co} was taken equal to 0.002 in the proposed equation.

$$\varepsilon_{cu} = \left(1.75 + 12\frac{f'_{lu}}{f'_c}\left(\frac{\varepsilon_{h,rup}}{\varepsilon_{co}}\right)^{0.45}\right)\varepsilon_{co} \tag{12}$$

2.4. Ilki Model

Stress-strain relationship of this model (referred as Ilki) was proposed for circular, square and rectangular sections and shown in Fig. 4 based on the studies of Ilki and Kumbasar [22] and Ilki et al. [21]. This model is similar to Lam and Teng model since both models considered the bilinear four-parameter equation suggested by Richard and Abbott [36]. In the proposed analytical model, polynomial constant (n) was taken equal to 20 by Ilki et al. [21] and for the transition of branches and strain reduction factor (k_ε) was as 0.700 for carbon FRP material in this model. Ultimate stress and strain of FRP-confined section $(f'_{cu}, \varepsilon_{cu})$ can be computed by Eqs. (13) and (14), respectively. In the equations, f'_{lu} is the effective confining stress. In the equation, ε_{co} is accepted as 0.002, b and h are the width and depth of member section, respectively.

$$f'_{cu} = \left(1 + 2.4\left(\frac{f'_{lu}}{f'_c}\right)^{1.2}\right) f'_c \tag{13}$$

$$\varepsilon_{cu} = \left(1 + 20\frac{h}{b}\left(\frac{f'_{lu}}{f'_c}\right)^{0.5}\right)\varepsilon_{co} \tag{14}$$

2.5. Mechanical attributes of materials

In the study, two different reinforcement materials notated as S220 and S420 which has yield strength (f_{sy})of 220 MPa and 420 MPa is used for the determination of numerical cross-sectional dimensions, respectively. Strength and strain capacity of reinforcing materials are provided in Table 1 as suggested in TBEC [37]. Young modulus (E_s) of both materials was equal to 200 MPa.

It was assumed that all generated cross-sections are laterally confined with CFRP. Attributes of CFRP material was taken from Lam and Teng [19,20] compatible with ACI 440 [31] and modulus of elasticity (E_j) was 235 GPa and tensile strength (f_{ju}) of CFRP was 3530 MPa.

3. Validation of numerical models with experimental study

In the study, stress-strain relationship of all FRP models coded in spreadsheet software in Excel and axial-load-moment and moment-curvature analysis were performed. To validate the adopted stress-strain models and developed software, experimental studies of Iacobucci et al. [38] was used to compare the results of numerical models adopted in this study. All column dimensions in the

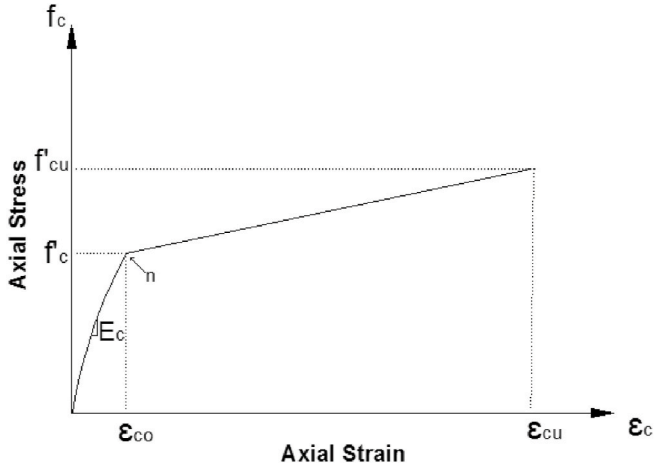

Fig. 4. Stress-strain relationship for Ilki et al. (2004).

Table 1
Strength and strain properties of reinforcing bars given in TBEC.

Type	f_{sy} (MPa)	ε_{sy}	ε_{sh}	f_{su} (MPa)	ε_{su}
S220	220	0.0011	0.011	264	0.12
S420	420	0.0021	0.008	504	0.08

experiment were 305 × 305mm, section reinforcement layout is shown in Fig. 5 and properties of member and loading values in the experiment is given in Table 2. Detailed information about the experimental program can be found in the related study.

It can be seen from Table 2 that thickness of CFRP and axial load on the cross-sections was changed, and also relatively close but different unconfined concrete strength values was considered in the experiment. In the experiments, stirrup spacing was 300 mm, yield strength of lateral reinforcement was 457 MPa, and longitudinal reinforcement strength was 465 MPa. Iacobucci et al. [38] indicated that elastic modulus and tensile strength of CFRP was 76350 MPa, and 962 MPa/layer, respectively.

For validation purposes, five different samples of experiments were used and moment-curvature relation of sections with aforementioned attributes was obtained and compared with each experimental results as shown in Fig. 6. It can be seen from the figure that there is a good agreement between experimental and numerical models. In general, moment capacities of existing models around the balanced behavior where yielding occurs in tensile reinforcements, is comparable with experiments. It is observed that curvature values around the yield were overestimated for ASC-4NS in all models although moment capacities are well-predicted. Nevertheless, figure clearly shows that all models have superior performance in predicting bending capacity of members. Similarly, curvature capacity at yield and ultimate is fairly good in all models. It is observed that in some experimental samples, ultimate curvature capacity obtained from Pantelides model is higher than other models and experimental results. It should be noted that detailed quantitative assessment with existing models is also made in Section 5.3 using statistical parameters including moment-curvature response produced by proposed stress-strain relation model in this study.

During moment-curvature analysis, a neutral axis is assumed every value of curvature using section-fiber model. The strains of each fiber and reinforcing steel were obtained based on strain-compatibility. The strains corresponding to regarding constitutive model of FRP-confined concrete and reinforcing steel were determined to obtain the stresses. The stresses are then integrated to get the value of force contribution from each component in compression and tension. If the equilibrium of compressive, tensile and the axial load was within identified tolerance, then the moment from all fibers was summed and section moment at that curvature was obtained. Based on this moment-curvature analysis, it was possible to determine each N and M pairs and hence the N-M interaction diagram for comparison. N-M interaction of FRP-confined members with experimental results (N-M points) provided by Rocca et al. [39] using Iacobucci et al. [38] experiments were used and compared with N-M diagram obtained by developed software program. In Fig. 7, N-M diagrams were obtained and drawn by developed software and N-M points were taken from each sample experiments. It can be observed Youssef and Pantelides models slight underestimated the moment capacities for ASC-2NS while Ilki and Lam and Teng models were compatible. As also observed from moment-curvature response, all model predictions were relatively lower than experiments and this situation can be also apparently seen in Fig. 7 for ASC-6NS specimen. Moment capacities determined from Ilki and Lam ang Teng models have agreement while other models produced lower values for the moment capacity of ASC-5NS specimen. As seen in Fig. 7, moment capacity produced by Pantelides model is more compatible while moment capacity of Youssef model was low and moment produced by Ilki and Lam and Teng models were slightly higher for ASC-4NS specimen. It can be stressed that N-M diagrams especially observed for experiments have similar trends naturally and compatible with moment-curvature responses since these responses were determined for given axial loads given in Fig. 6 and Table 2. Finally, it can be claimed that that developed spreadsheet software is capable of obtaining accurate results considering satisfactory compatibility with experimental results.

4. Construction of analytical sections and evaluation analysis

Determining the validity of numerical results for computation of stress-strain and moment-curvature capacity of experimental results, numerous analytical sections to cover broad range of concrete members were constructed. By this way, efficiency of CFRP using different section parameters such as member dimensions, axial load level, longitudinal reinforcement ratios, transverse reinforcement layouts will be scrutinized. Generated RC sections will be also analyzed as-built using confined and unconfined concrete model [33] for comparison purposes. In addition, effect of these parameters on the stress-strain, moment-curvature, N-M diagram of members and their dependency on CFRP will be investigated.

All generated RC section was confined with thickness (t_j) of 1 mm of CFRP material and it was assumed that all RC sections were

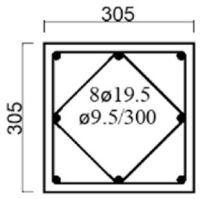

Fig. 5. Cross-section and reinforcement layout from experimental program of Iacobucci et al. [38].

Table 2
Characteristics of experimental study Iacobucci et al. (2003).

Sample name	f_c' (MPa)	t_j (mm)	N (kN)
ASC-2NS	36.5	1	1290.3
ASC-3NS	36.9	2	2231.2
ASC-4NS	36.9	1	2231.2
ASC-5NS	37.0	3	2237.3
ASC-6NS	37.0	2	1307.9

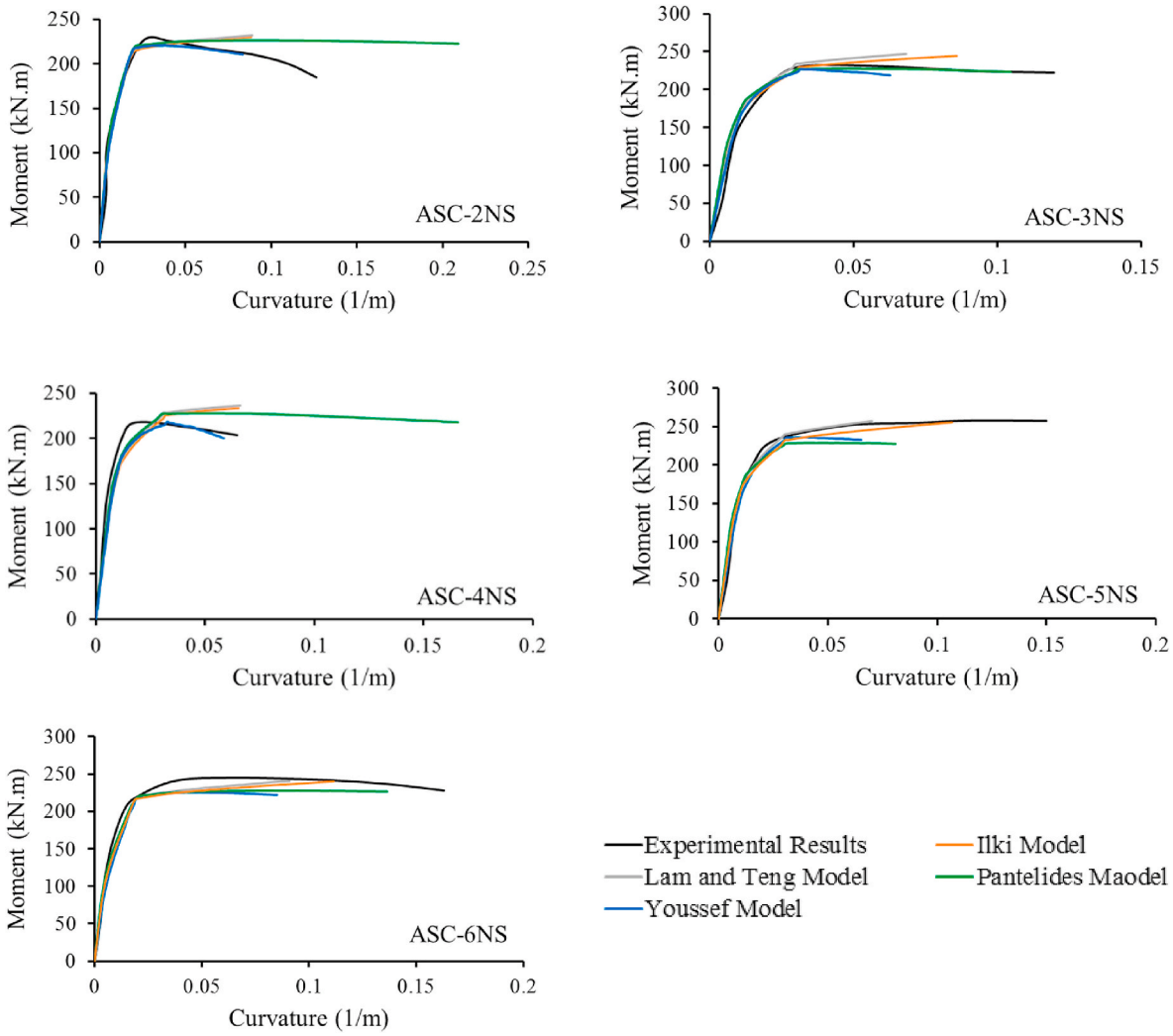

Fig. 6. Comparison of moment-curvature relation between numerical models and experiment.

laterally confined using different FRP models given Section 2. Corner radius (r_c) was assumed 25 mm and diameter of stirrup was taken constant and 8 mm in all FRP-confined RC sections. In the study, square and rectangular sections were used, and depth/width of RC section were taken 0.5, 1.0 and 2.0. Axial load ratio ($\upsilon = N/bhf_c'$) RC sections were taken between 0 % and 50 % with increments of 10 %. To investigate effect of CFRP on the strength and deformation of RC sections, unconfined concrete strength (f_c') was altered between 10, 16, 25 and 30, 40 and 50 MPa to represent low- and medium-strength concrete. Longitudinal reinforcement ratio (ρ_l) of members was taken between 1 % and 4 % with increments of 1 %, strength of longitudinal and transverse reinforcement (f_{sy}) was considered as in Table 1 and stirrup spacing (s) was altered as 100 mm and 200 mm.

4.1. Evaluation of analysis results

In this section, analysis results are evaluated in three ways: 1) stress-strain relationship of FRP models are evaluated of square and

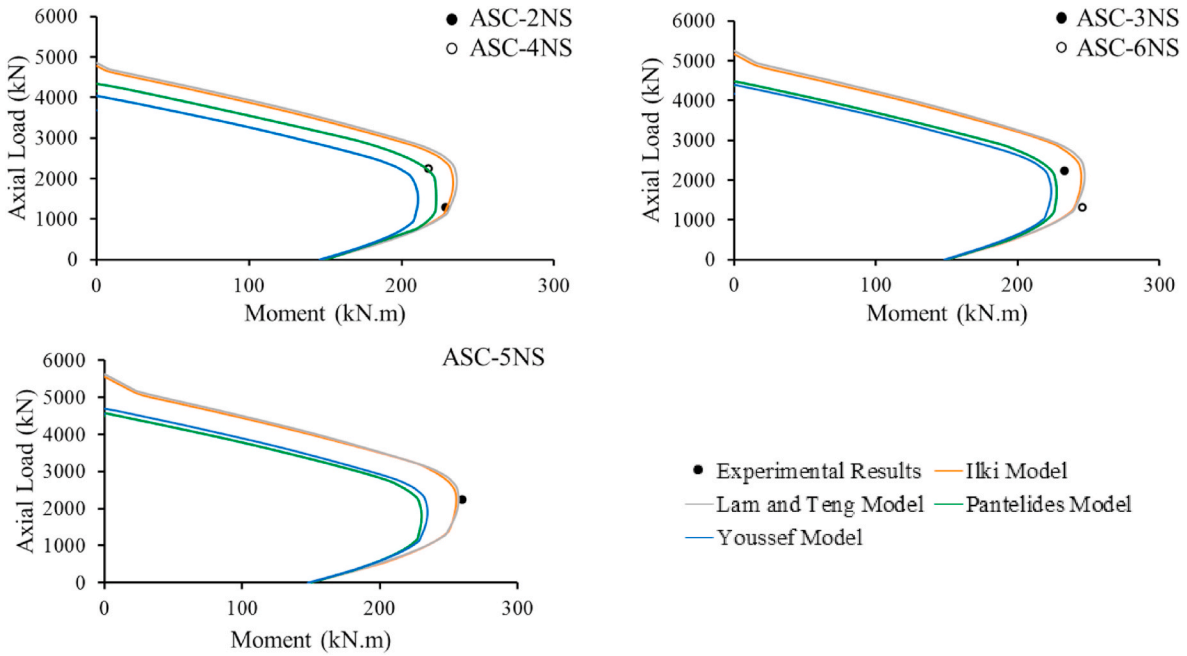

Fig. 7. Comparison of numerical models with experimental results considering N-M diagram.

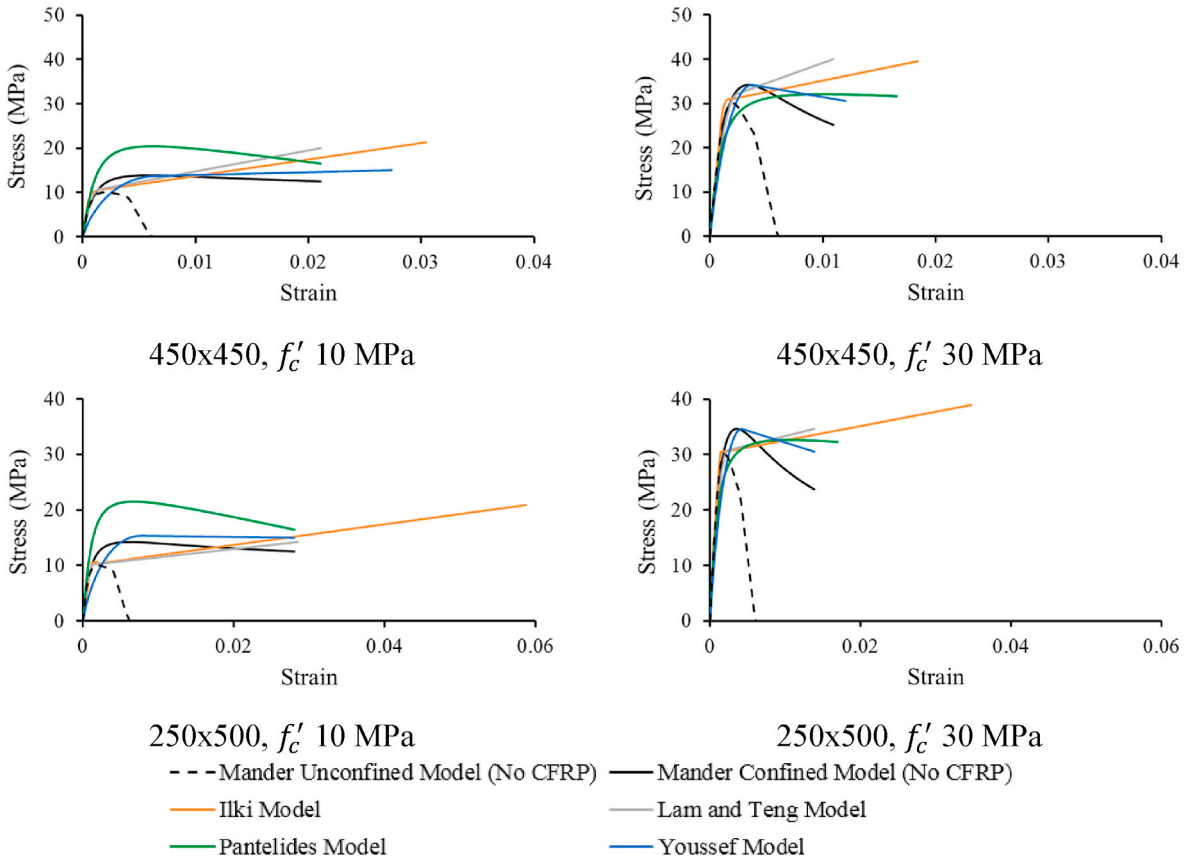

Fig. 8. Comparison of concrete models in RC sections with h/b ratio of 1 and 2.

rectangular section considering different unconfined strength of concrete, 2) moment-curvature capacity of members used for different υ and ρ_l to compare FRP models, 3) N-M diagram of FRP models were compared.

Unconfined concrete strength of 10 MPa and 30 MPa are used to compare $\sigma - \varepsilon$ relation of FRP-confined, and ordinary confined and unconfined concrete models. For comparison purposes, $f_{sy} = 420$ MPa, $s = 100$ mm and $\rho_l = 1\%$ is assumed to compute confined concrete stress-strain relation. Due to the presence of stirrups in RC sections, it was evaluated that the ultimate capacity of FRP-confined section would not be less than Mander et al. [33]. As an example, comparison of stress-strain relation for square (450 × 450 mm) and rectangular sections (250 × 500 mm) are shown in Fig. 8.

It can be seen from the figure that all FRP models quite improved $\sigma - \varepsilon$ relation of concrete compared to unconfined model. When the results are evaluated for square section, it can be said that the compressive strength increase between FRP models can be listed as Ilki, Pantelides and Lam Teng model compared to confined concrete model in the case of $f_c^{'} = 10$ MPa. Increase in the strength observed quite low in Youssef model. If the improvement of ultimate strain ε_{cu} is compared, it can be said that Youssef and Ilki provided higher ultimate strain and hence the ductility compared to other models. The highest increment for high strength case $f_c^{'} = 30$ MPa is observed from Ilki and Lam and Teng model and ultimate strength of both models is almost similar. Ilki Model approximated the

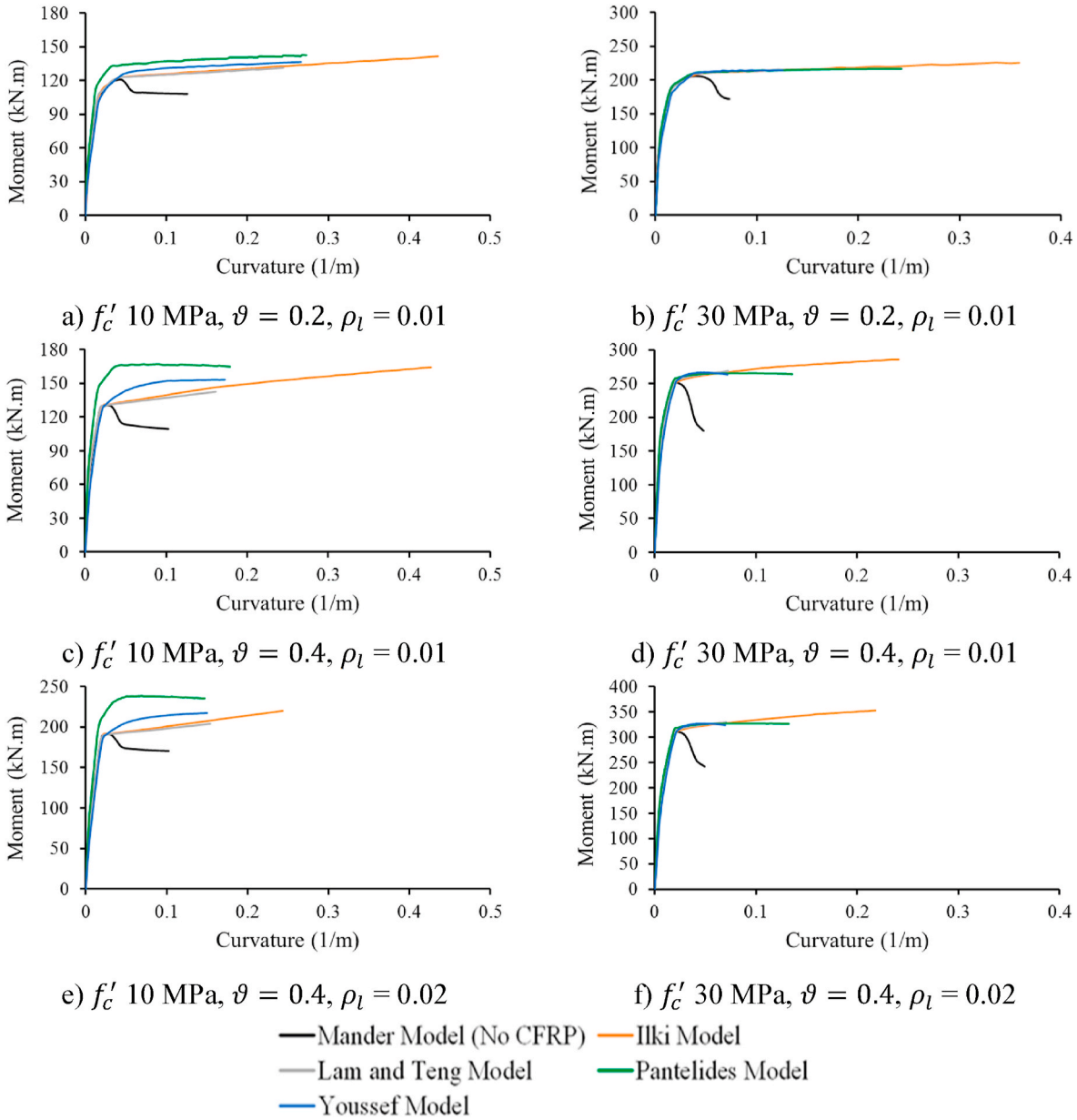

Fig. 9. Moment-curvature relation of 600x300 section and comparison of as-built and FRP models.

highest ultimate strain, and it is followed by the Pantelides and Youssef models. For rectangular sections, it was observed that Ilki model produced the highest strength and ultimate strain values compared to other models and this is not dependent to unconfined concrete strength. Pantelides model also provided high stress values with Ilki model especially for $f_c' = 10$ MPa. If both square and rectangular section considered together, it can be said that Ilki model considerably higher than other models in terms of stress and strain values and it is expected high strain values will result higher deformation capacities.

In the second way of evaluation of FRP models, moment-curvature capacity of sections was used and compared. RC column with 600 × 300 mm section dimensions that have 420 MPa yield strength capacity of reinforcement is considered for comparison and moment-curvature capacity of all FRP models are drawn in Fig. 9 using different ρ_l, υ and f_c'. It can be seen from the figure that moment capacity of section is increasing with increasing ρ_l as seen from Fig. 9c–e and Fig. 9d–f. In the study, columns were subjected to maximum 40 % of axial load capacity and hence columns behaved around or below the balanced behavior. Accordingly, moment capacity of columns increased with increasing axial load ratio and this situation can also be observed if Fig. 9a–c and Fig. 9b–d are compared. In addition, moment capacity of RC members was higher for high strength concrete material as observed in Fig. 9a–b, c-d and e-f. This situation is valid for as-built RC sections and FRP-confined columns. When the effect of CFRP is observed, figures clearly indicates that deformation capacity of FRP-confined sections are dramatically increased compared to as-built RC sections. When the bending capacity of RC section is compared, it can be said that moment capacity of CFRP sections is increasing after yield and stiffness of members is positive beyond this level. This situation is also compatible with $\sigma - \varepsilon$ behavior of FRP-confined sections. Fig. 9b–d and f also demonstrate that moment capacity of RC sections are almost identical at yield regardless of FRP model. However, bending capacity of section may be diverged between the FRP models and hence, it is not similar for low-strength concrete. In addition, the difference between the models becomes more apparent with increasing ρ_l and υ. In general, Pantelides and Youssef models produced higher bending moment capacities and Ilki and Lam Teng models were almost identical. This situation highlighted that bending capacity of FRP-confined RC section could be diversified especially for low strength concrete. Evaluations have indicated that moment-curvature trend of Lam Teng and Ilki models are almost identical, and it is thought that this could be due to similar $\sigma - \varepsilon$ relation of both models. On the other hand, curvature capacities produced from Ilki model are considerably higher than Lam and Teng model, compatible with $\sigma - \varepsilon$.

In third evaluation approach, N-M diagram of as-built and FRP-confined RC sections are investigated considering 400 × 400 mm and 250 × 500 mm as an example. Comprehensive statistical evaluations will be also made for all generated sections following this section. N-M diagrams are drawn for $f_c' = 25$ MPa, $f_{sy} = 420$ MPa considering $\rho_l = 1\%$ and $\rho_l = 4\%$ separately in Fig. 10. It can be observed from the figure that moment capacity of FRP-confined sections significantly higher than as-built RC sections especially at

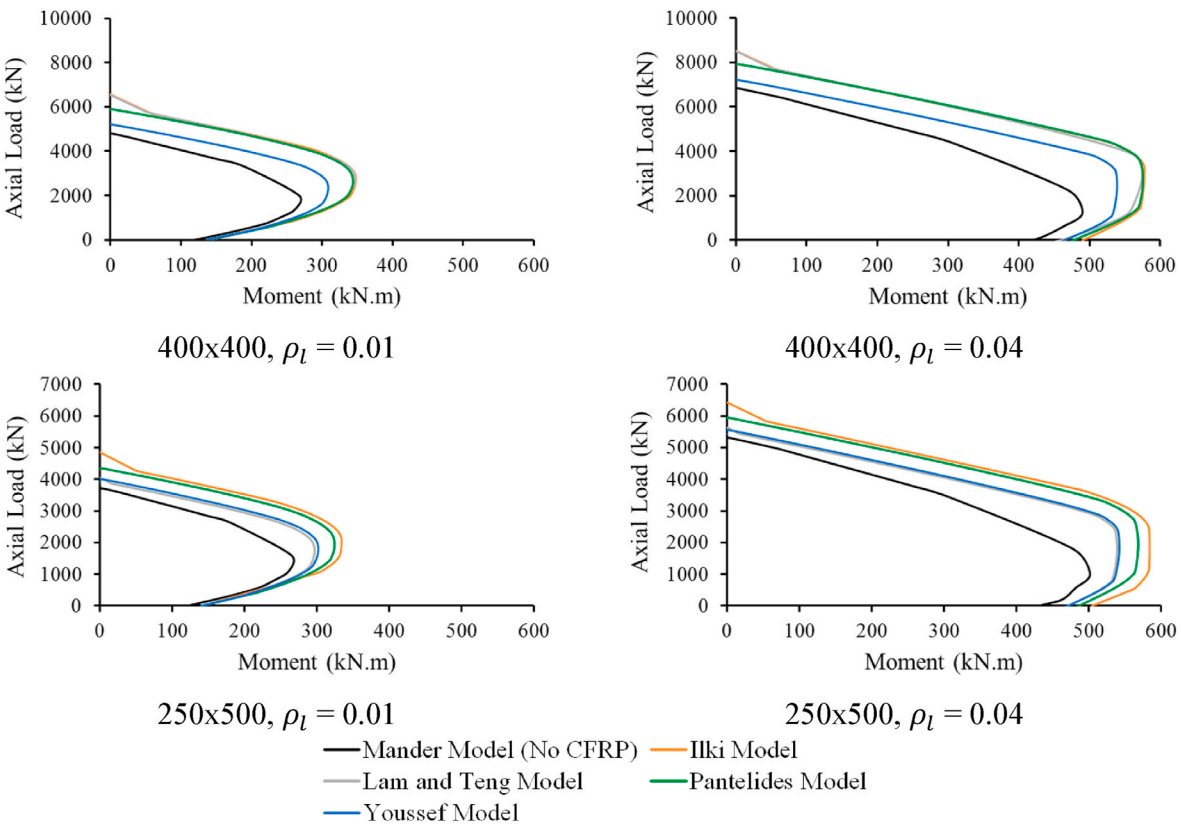

Fig. 10. N–M diagram comparison of as-built and FRP-confined RC square and rectangular sections.

high axial load levels. Around the balanced behavior and below this level, effect of CFRP is decreasing on the strength and member moment capacities gets quite close. Nevertheless, CFRP effect on the member strength can be apparently seen at high longitudinal reinforcement ratio $\rho_l = 4\%$. This situation is valid for both square and rectangular sections. N-M diagrams obtained from both section dimensions also indicated that balanced behavior of members is extended to higher axial load levels especially for $\rho_l = 4\%$ compared to as-built RC sections.

When the effect CFRP models is compared, it can be said that Ilki and Pantelides models produced higher moment capacities for sample square and rectangular sections, and this is valid for almost all axial load levels and longitudinal reinforcement ratios. In general, Youssef and Lam and Teng models produced lower moment capacities for both sections. It seems from the figure that Lam and Teng model produced higher moment capacities than Youssef model especially at high axial load levels for 400 × 400 mm square section while Lam Teng model generally produced equal or lower moment capacities than Youssef model in low axial load ratios ($\upsilon \leq 20\%$). It is worth to note that obtained N-M diagrams are discussed just for sample sections and effect of f_c' cannot be observed from Fig. 10 since effect of CFRP was not clearly observed for high f_c' values as shown earlier. Accordingly, detailed statistical analysis will be made to evaluate effect of CFRP on moment and deformation capacities of RC section using wide range generated RC sections.

4.2. Statistical assessment of analysis results

In this section, influence of CFRP on the capacity of RC sections were statistically scrutinized by statistical analysis accounting numerous derived analytical sections since small partition of these sections were compared in earlier sections. To assess the development of stress-strain behavior of unconfined concrete, the stress and strain ratio of FRP-confined sections at ultimate were divided to the corresponding unconfined concrete stress and strain values. By this way, the ratio of increment in terms of strength and deformation capacity of unconfined concrete were obtained and compared for different FRP models. In addition to stress-strain relations, the effect of CFRP on the curvature capacity of RC sections were analyzed. For this purpose, ultimate curvature capacity of as-built RC sections and FRP-confined sections were obtained from moment-curvature analysis and curvature values were divided to determine development in sectional capacities.

In Fig. 11, the ratio of stress and strain of CFRP to unconfined concrete was computed for a sample 400 × 400 mm squared section and distribution of ratios were plotted against f_c'. It can be seen from the figure that significant development was obtained for low-strength concrete depending on the FRP model and development is gradually decreasing with increasing concrete strength. The similar trend was also observed for strain development of unconfined concrete in all FRP models except Pantelides model. According to Pantelides model, effect of FRP confining is increasing with increasing concrete strength. Since some models account the existence of longitudinal reinforcement ratios, the ratios for different longitudinal reinforcement ratios were plotted to investigate the effect of this parameter. In Fig. 11, different hallow circles for the same FRP model represents the effect of longitudinal reinforcement ratio. It can be said that effect of this parameter is very limited both on stress and strain development as can be also seen from the distribution of circles. The results of rectangular sections were not drawn to eliminate the repetition of figures. Nevertheless, it can be said that that similar trends against f_c' are also valid for rectangular sections. All analytical sections will be also further compared and evaluated statistically.

In addition to development of materials, development of curvatures at section level is investigated. For this purpose, a sample as-build and FRP-confined squared section (400 × 400 mm) with $\rho_l = 1\%$ is used and ultimate curvature values obtained from moment-curvature analysis were divided to determine curvature development of corresponding RC section and results were plotted in Fig. 12 according to f_c' and axial load ratio ($\upsilon = N/bhf_c'$). Fig. 12a shows that curvature development of different FRP models against f_c' and it can be claimed that FRP confining significantly increases the curvature capacity compared to as-built section. Trend of numerical models may differ according to f_c' and it seems that ratios are increasing in Ilki and Pantelides models with increasing unconfined concrete strength while this is reversed in Lam&Teng and Youssef models. In Fig. 12a, effect of axial load ratio cannot be clearly observed, and to evaluate the effect of axial load ratio on the curvature response development Fig. 12b is plotted. Fig. 12b indicates

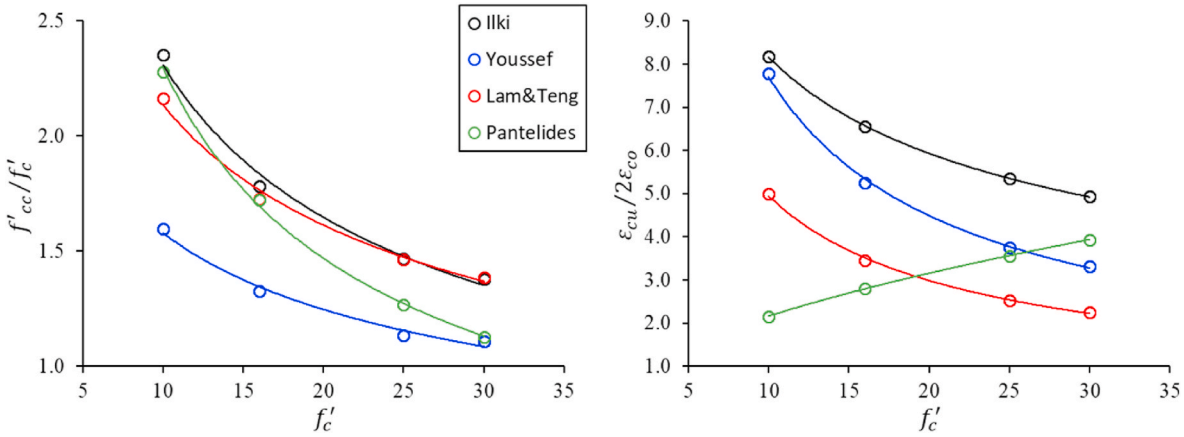

Fig. 11. Stress and strain versus f_c' development distribution for a sample squared (400 × 400 mm) section.

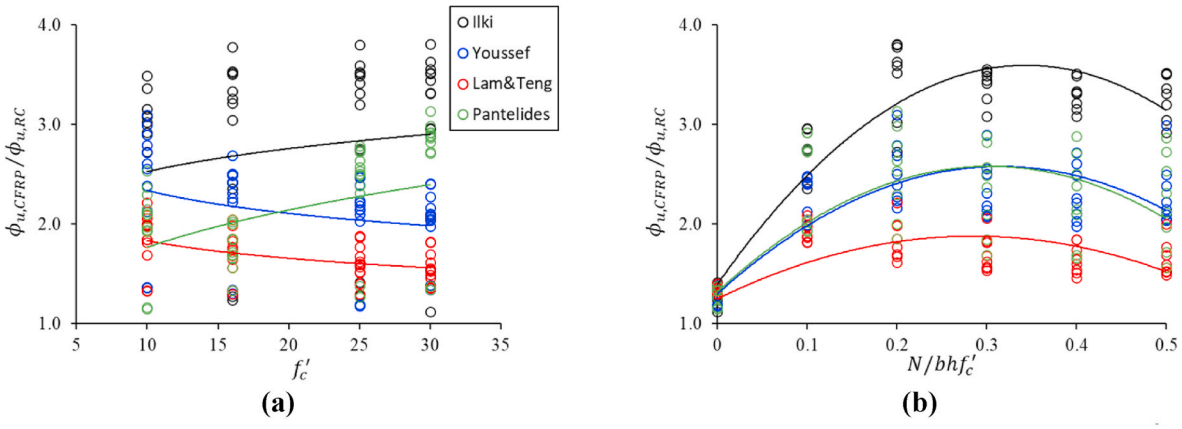

Fig. 12. Curvature development of as-built sample squared (400 × 400 mm) section according to f_c' and axial load ratio.

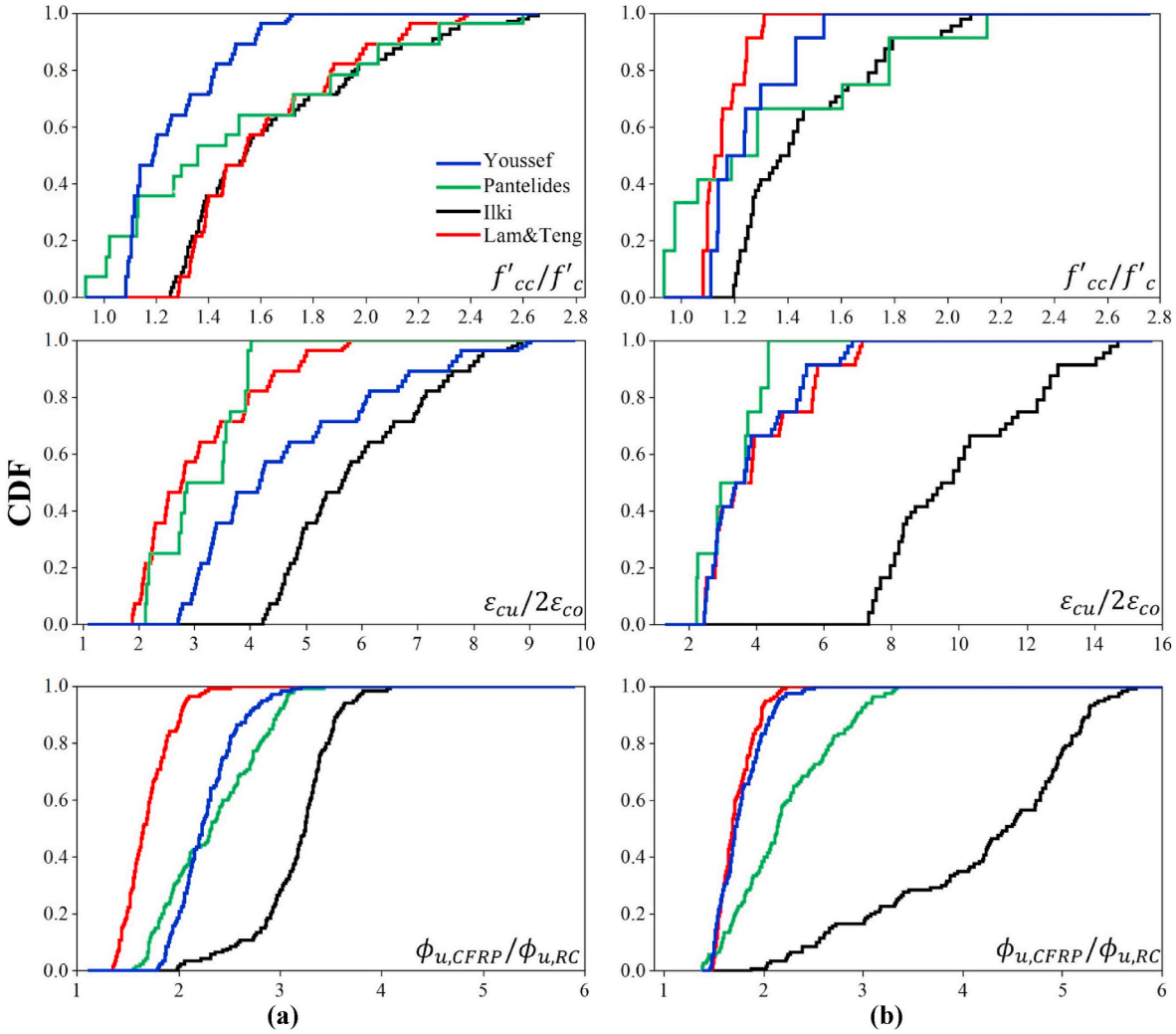

Fig. 13. Cumulative distribution function for all RC sections in development of strength, ultimate strain and curvature capacity for a) Square b) Rectangular sections.

that efficiency of FRP confining is increasing at higher axial load ratios.

Developments in stress, strain and curvatures capacities were made for a sample section in above paragraphs. To evaluate all analytical results, computations were further made for all models and sections, and cumulative distribution function (CDF) of results for all section types were compared and evaluated in Fig. 13. In the figure, development of strength, ultimate strain and curvature capacity of square (left) and rectangular (right) sections are provided separately.

It can be seen from the figure that different models produced different strength and ultimate strain values for both section types. In general, Ilki model provided higher strain values compared to other models. Since higher strain values determined from this model, higher curvatures were also obtained from Ilki model. This situation can be more apparently seen in rectangular sections. In general, other models are comparable and may produce different strain values for square and rectangular sections. It can be also stated in both section types, curvature responses determined from Lam and Teng model is slightly lower than other models. Lam and Teng produced almost similar values in terms of strength with Ilki model, but due to lower ultimate strain values, curvature capacity of Lam and Teng model was lower than Ilki model. Youssef model produced lower strength values compared to Lam and Teng model, but higher ultimate strain values were for Youssef model. Accordingly, ultimate curvature capacity of Youssef model was higher than Lam and Teng model.

5. Prediction equations for stress and strain at ultimate

Based on the statistical analyses given in section 4.2, simplified backbone curve and prediction equations for FRP-confined RC sections at ultimate levels, are developed by adapting Lam-Teng model. During the development of equations, ultimate stress and strain values of Lam&Teng model is also considered due its simplicity, wider acceptance in the literature, consideration of various parameters including section geometry, dimensions and material compared to other FRP model. In addition, Lam&Teng model was preferred since strain and stress values produced by this model is slightly conservative than other models.

In previous section, all analysis were performed for $r_c = 25mm$, $f_{ju} = 3530$ MPa and $k_\varepsilon = 0.586$ for CFRP material and h/b ratio was between 0.5, 1.0 and 2.0. On the other hand, parameters used in the analyses can be varied depending on the material content, section dimensions, etc. and various values for these parameters can be found in the literature [9,23,31,40]. Considering this issue, various values for these parameters are used and r_c is taken between 25 mm and 50 mm with increments of 5 mm. Extreme values for f_{ju} and k_ε provided in ACI 440 [31] is used and they range around 700 MPa–3600 MPa, and 0.4 to 1.0, respectively. Accordingly, f_{ju} taken between extreme values with increments of 700 MPa (700, 1400, 2100, 2800 and 3500 MPa), and k_ε with increments of 0.2 (0.4, 0.6, 0.8 and 1.0). In addition to these parameters, sections dimension ratios are increased and sections dimension of 3 and 4 is added. Consequently, RC sections with h/b ratios of 0.5, 1.0, 2.0, 3.0 and 4.0 is considered. Regarding all parameters such as $h/b, \rho_l, r_c, f_{ju}, f'_c$ and k_ε, more than 350,000 RC sections were analyzed and used for the development of prediction equations.

Proposed equations follow two different equation forms, namely, linear $(y = ax + b)$ and power $(y = ax^b)$ functions as provided in Eqs. (15) and (16), respectively. Eq. (15) is used to predict ultimate confined stress, and Eq. (16) predicts the ultimate strain of FRP-confined concrete based on the regression analysis in previous section. It was found that proposed functional forms fit best to the available data. The left side of the equations is the ratio of predicted FRP ultimate stress to unconfined concrete stress, and FRP ultimate strain to unconfined concrete strain (i.e., $\varepsilon_{co} = 0.002$) the that compatible y-axis given in figures earlier, respectively. In the equations, ρ_j defines the volumetric ratio of FRP sheet as given in Eq. (17) [18,21], a_1, a_2 and b_2 are also defined as functions depending on the $h, b, h/b, \rho_l, r_c, f_{ju}, f'_c$ and k_ε parameters which functional form of both equations will be determined by statistical analysis. In Eq. (15), b_1 is constant and it is equal to unity.

$$\frac{f'_{cu}}{f'_c} = (a_1\rho_j + b_1) \tag{15}$$

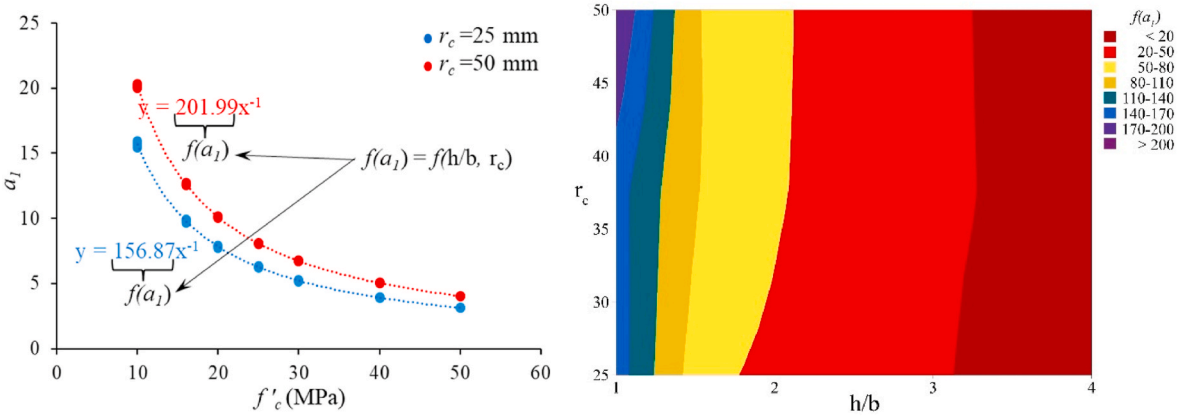

Fig. 14. The distribution of dependent variable (a_1) versus f'_c (Left) and h/b ratio (Right) defined in Eq. 15.

$$\frac{\varepsilon_{cu}}{2\varepsilon_{co}} = \left(a_2 \rho_j^{b_2}\right) \tag{16}$$

$$\rho_j = \frac{2t_f(b+h)}{bh} \tag{17}$$

5.1. *Prediction of ultimate stress for FRP-confined RC sections*

To expose the significant parameters on the correlation of strength capacities, effect of each parameter is studied. For this purpose, some parameters such as f_{ju} and k_ε were neutralized and the lowest values for these parameters were used (i.e., $f_{ju} = 700\ MPa$ and $k_\varepsilon = 0.40$) for correlation analysis. Later, these parameters were included in statistical analysis to evaluate final form of the equation. General form of proposed stress equation is based on the linear function and constant value (a_1) of dependent parameter (ρ_j) is investigated. Statistical analysis has shown that constant value can be also defined as a function of $h/b, r_c$ and f_c' as shown in Fig. 14. In Fig. 14a, the relation between a_1 and f_c' is plotted for $h/b = 1$. Fig. 14a shows that a_1 is inversely proportional to f_c' and it increases with increasing r_c. This observation is also valid for rest of h/b ratios, but a_1 values tend to decrease with increasing h/b as illustrated in Fig. 14b. Observations have shown that ρ_l has very limited effect on the correlations (see Fig. 14a) and effect of this parameter is omitted in statistical analysis for the sake of simplicity.

The other implication relation between a_1 and f_c' is that constant a_1 can be directly parametrized by h/b and r_c and this ease to describe relation of a_1 with these parameters as shown in Fig. 14b. Additional correlation analyses were carried for different function forms of h/b and r_c for a_1 and results demonstrated that power function can be used to relation between them.

In Fig. 15, typical relation between h/b, r_c and a_1 is plotted and it can be clearly said that power function fits well with actual data. The variables of this power function (m_1, m_2 and m_3) are determined via spreadsheet software developed by authors using Microsoft Excel. In addition, lower and upper limits of these variables are also provided for %95 confidence level as given in Table 3.

To determine the correlations and residual values between predicted and actual values, mean values of coefficients are used. Linear correlation analysis has shown that coefficient of determination (R^2) between predicted and calculated values is 0.99. Residual values (real-predicted) for mean coefficients are also shown in Fig. 15b and according to residual analysis, sum of squared errors (SSE) and root mean squared errors (RMSE) found quite low and around 40.34 and 1.39, respectively.

All statistical analyses above were performed for typical values of $f_{ju} = 700$ MPa and $k_\varepsilon = 0.40$, but it is known fact that these values may change depending on the material characteristics. Accordingly, effect of these parameters on the confined concrete strength should be also investigated. Considering the typical form of Eq. (15) for the prediction of strength, effect of these values on the a_1 is evaluated and results are plotted in Fig. 16. Regarding the obtained relation of f_{ju} and k_ε parameters with different values section dimensions, unconfined concrete strength etc., it can be claimed that both parameters have linear relation with a_1 as seen the power of equation for both figures. Consequently, these parameters were added as linear partition of Eq. (15) for a_1 based on the observed relations as provided in Eq. (18) and the lowest values for these parameters were used as denominator in the equation. To determine ultimate stress of RC section due to FRP confining, Eq. (18) should be placed in Eq. (15).

$$a_1 = 48.\left(\frac{k_\varepsilon}{0.4}\right).\left(\frac{f_{ju}}{700}\right).\left(\frac{1}{f_c'}\right).\left(\frac{h}{b}\right)^{-2.3}.(r_c)^{0.37} \tag{18}$$

5.2. *Prediction of ultimate strain for FRP-confined RC sections*

Statistical analyses were further made for the prediction of ultimate strain of FRP-confined section analytically. For this aim, $\varepsilon_{cu}/2\varepsilon_{co}$ ratios were investigated in terms of mathematical function given in Eq. (16). For this purpose, section that represent the different materials of FRP was selected and relation is plotted in Fig. 17. The figure is drawn for $h/b = all$, $r_c = 25$ mm and $f_c' = 10$ MPa by changing the f_{ju} and k_ε values for each figure. According to figure, it was observed that Eq. (16) may lost its reliability especially for higher ρ_j ratios depending on the material quality. Nevertheless, evaluations also indicated that strong correlations can be obtained by

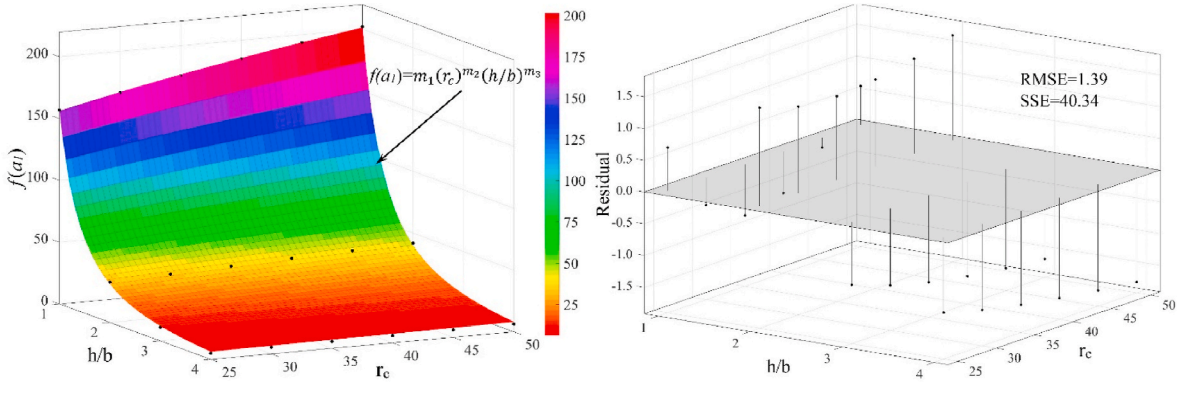

Fig. 15. The functional form (Left) and residual values (Right) for optimal values of the developed equation of a_1 against h/b and r_c.

Table 3
Values of power function variables for a_1.

m_1	m_2	m_3
48 ± 5 (43, 53)	0.37 ± 0.30 (0.34, 0.40)	−2.3 ± 0.1 (−2.2,-2.4)

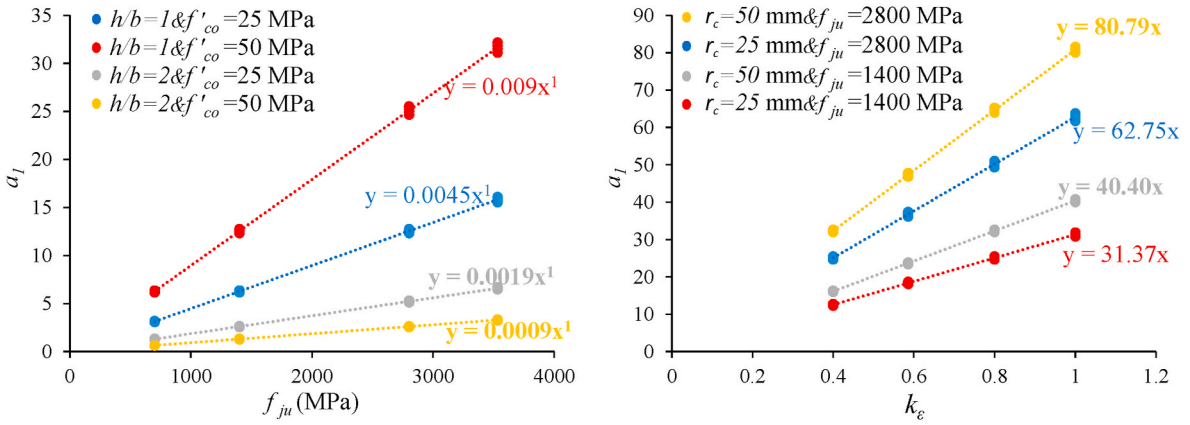

Fig. 16. The relationship and correlation of a_1 versus f_{ju} (Left) and k_ε (right).

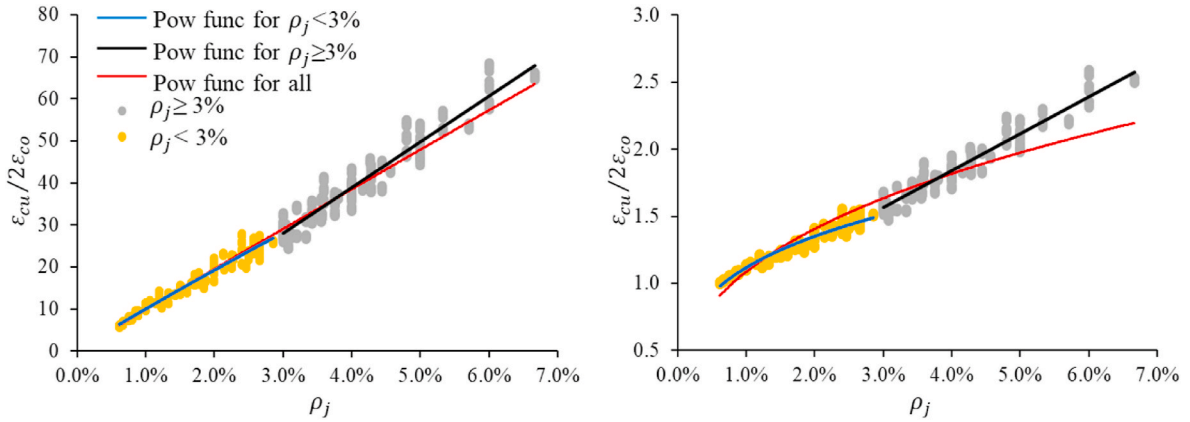

Fig. 17. $\varepsilon_{cu}/2\varepsilon_{co}$ versus ρ_j (left: $f_{ju} = 3510$ MPa & $k_\varepsilon = 0.4$; right: $f_{ju} = 700$ MPa & $k_\varepsilon = 1.0$).

splitting the equation by means of FRP volumetric ratios. Based on the statistical assessments, it was determined that higher correlation could be obtained for $\rho_j < 3\%$ and $\rho_j \geq 3\%$. In Fig. 17, blue, black and red continuous lines represent the effect of power function considering $\rho_j < 3\%$, $\rho_j \geq 3\%$ and $\rho_j = all$. It can be said that separation of equation regarding ρ_j is effective to represent relation $\varepsilon_{cu}/2\varepsilon_{co}$ versus ρ_j.

According to these results, two different versions of (a_2, b_2) variable pairs should be obtained for divided ρ_j to predict ultimate strain of FRP-confined RC sections. It is certain that these pairs will be also dependent on parameters such as $h/b, r_c, f_{ju}, k_\varepsilon$ and f_c' as was observed in the determination strength of FRP RC section. In Eq. (19), possible mathematical form of (a_2, b_2) variable pairs are given. These pairs are constants of power functions, and they can be obtained by further statistical analysis.

$$(a_2, b_2) = \begin{cases} If\ \rho_j \geq 3\%\ then & f\left(h/b, r_c, f_c', f_{ju}, k_\varepsilon\right) \\ If\ \rho_j < 3\%\ then & f\left(h/b, r_c, f_c', f_{ju}, k_\varepsilon\right) \end{cases} \tag{19}$$

To reduce the effect of unknown parameters, f_{ju} and k_ε parameters were excluded from statistical analyses, and they were used as fixed variables Evaluations also highlighted that f_{ju} and k_ε parameters linearly influenced the $\varepsilon_{cu}/2\varepsilon_{co}$ distributions and hence, these parameters can be subsequently added to Eq. (18). For this reason, efficiency of $h/b, r_c$ and f_c' parameters were investigated by the lowest values of f_{ju} and k_ε for each (a_2, b_2) variable pairs separately. In Fig. 18, effects of $h/b, r_c$ and f_c' parameters are drawn for each

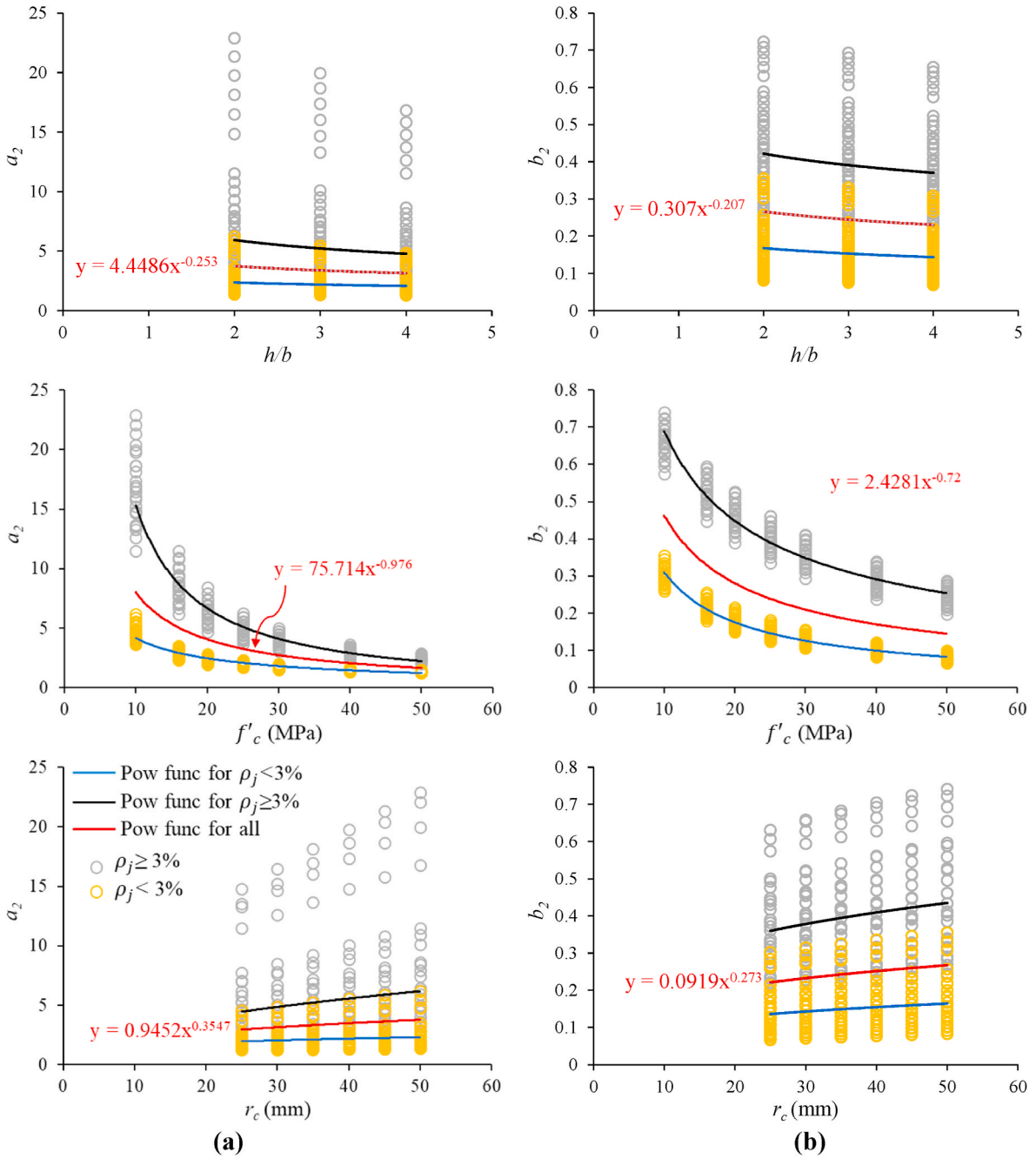

Fig. 18. Effect of various parameters on the distribution of (a) constant a_2 and (b) power b_2 for Eq. (16) considering $f_{ju} = 700$ MPa and $k_\varepsilon = 0.4$.

variable to identify functional form. In Fig. 18, the distribution of a_2 and b_2 variables did not plot for $h/b = 1$ since unity does not have any statistical inference owing to mathematical form of power function.

In the figure, hallow circles represent the change of a_2 and b_2 variables for rectangular sections considering different ρ_{FRP} ratios. Power functions were used to show relation of a_2 and b_2 variables and red continuous line was drawn considering all sections and variable of the function is given in red. It can be seen from the figure that a_2 and b_2 variables are inversely proportional to h/b and f_c' parameters while directly proportional to r_c parameter. It can be also said that separation of variables in terms of ρ_j ratios seem reasonable and difference between the relations can be observed. This situation was seen in f_c' parameter more apparently.

The relations of $h/b, r_c$ and f_c' parameters with a_2 and b_2 variables plotted in Fig. 18 was used to combine effect of these parameters to obtain parametric equations. According to relations seen in Fig. 18, minimum, maximum and average values for the power function were used as basis for this parametric equation. For example, the relation a_2 with r_c for all RC section indicates that average constant

values of power function are 0.9452 and 0.3547. To simplify the equations between the parameters (i.e., $h/b, r_c$ and f_c') and variables a_2 and b_2, only exponent were considered such as 0.3547 for previous example because proportion between these parameters could be determined for the equations. Using the spreadsheet software developed by authors using Microsoft Excel solver, Eqs. (20) and (21) were determined and notated as a_2' and b_2'. These notations were used to represent the virtual values of a_2 and b_2 variables since square sections ($h/b = 1$) were not considered for the derivation of these equations.

$$a_2' = \left(\frac{k_\varepsilon}{0.4}\right).\left(\frac{f_{ju}}{700}\right).\begin{cases} If\ \rho_j \geq 3\%\ then & (h/b)^{-0.25}.(r_c/25)^{0.4} \Big/ (f_c'/10)^{0.7} \\ If\ \rho_j < 3\%\ then & (h/b)^{-0.20}.(r_c/25)^{0.25} \Big/ (f_c'/10)^{0.7} \end{cases} \tag{20}$$

$$b_2' = \left(\frac{k_\varepsilon}{0.4}\right).\left(\frac{f_{ju}}{700}\right).\begin{cases} If\ \rho_j \geq 3\%\ then & (h/b)^{-0.25}.(r_c/25)^{0.6} \Big/ (f_c'/10)^{0.7} \\ If\ \rho_j < 3\%\ then & (h/b)^{-0.20}.(r_c/25)^{0.25} \Big/ (f_c'/10)^{0.7} \end{cases} \tag{21}$$

To describe fully functional mathematical equation, the relation of Eqs. (20) and (21) with a_2 and b_2 variables should be introduced. For this purpose, these equations were applied to all created RC sections in the database and relation between them is plotted in Fig. 19. Naturally, relations between the parameters were diversified for square and rectangular sections. In the figure, relations of square section are plotted in hallow circles while hallo square shape for rectangular sections. Different colors were used to represent distinct ρ_j ratios. When the relations are investigated, it can be said that a_2 and a_2' is almost proportional, cross-sectional dimensions of sections have crucial effect and relations resemble the power function. However, section dimension effect is minimal and the relation of b_2 and b_2' is like elastoplastic behavior; relation is proportional in the first branch and none in second branch since increment of b_2' did not resulted the changes in b_2. Accordingly, the relation between them can be described as one-parameter sigmoid function.

Based on the definitions and relation of both parameters given in Fig. 19, final form of a_2 and b_2 variables can be obtained as defined in Eqs. (22) and (23). It can be seen from the equations that these parameters are conditioned to section geometry (e.g., square or rectangular) and volumetric FRP ratio (ρ_j). These equations also have some variables ranging m_4 to m_{13} that must be determined according to statistical analysis. It is worth reminding that before the calculation of Eqs. (22) and (23), a_2' and b_2' variables provided in Eqs. (20) and (21) should be calculated. The results of Eqs. (22) and (23) should be placed into Eq. (16) to predict the ultimate strain value of FRP-confined RC sections. Doing the statistical analysis, mean and %95 confidence bounds for the variables ranging from m_4 to m_{13} is provided in Table 4.

$$a_2 = \begin{cases} If\ \rho_j \geq 3\%\ then & m_4.(a_2')^{m_5} \\ If\ \rho_j < 3\%\ then & m_6.(a_2')^{m_7} \end{cases} \tag{22}$$

$$b_2 = \begin{cases} If\ \rho_j \geq 3\%\ then & m_8 - m_9.\left(e^{m_{10}.(b_2')}\right) \\ If\ \rho_j < 3\%\ then & m_{11} - m_{12}.\left(e^{m_{13}.(b_2')}\right) \end{cases} \tag{23}$$

5.3. Validation of the developed FRP-confined concrete model

In this section, prediction equations given in Eqs. (15) and (16) were applied to generated analytical sections. During the calculations, mean values of variables for the corresponding prediction equations is used (see Tables 3 and 4). The distribution of calculated values with real ones is plotted in Fig. 20. According to figure, correlation coefficient (R^2) for stress and stress ratios are 0.99 and 0.97, respectively. High correlations clearly indicate the accuracy of prediction equations with analytical ones. In addition to correlation

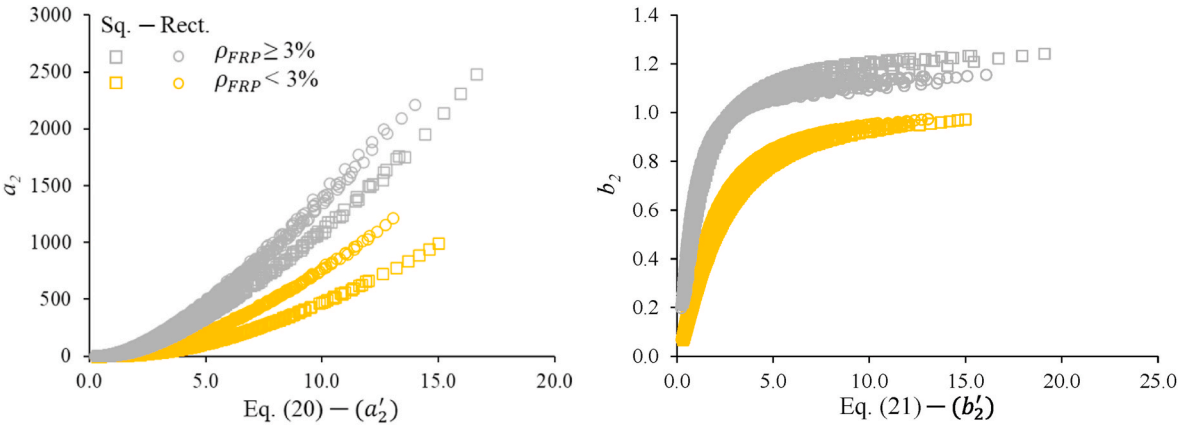

Fig. 19. Comparison of relation between parameters (a) a_2 and a_2' (b) power b_2 and b_2'.

Table 4
Mean and 95 % bound for the variables given in Eqs. (22) and (23)

Variables	Mean ± 95 % bounds Square (Rectangular)
m_4	24 ± 0.350 (33 ± 0.330)
m_5	1.66 ± 0.006 (1.62 ± 0.005)
m_6	4.85 ± 0.090 (9.3 ± 0.100)
m_7	1.98 ± 0.008 (1.92 ± 0.005)
m_8	1.2 ± 0.004 (1.1 ± 0.002)
m_9	1.1 ± 0.011 (1.0 ± 0.007)
m_{10}	−0.62 ± 0.011 (−0.8 ± 0.010)
m_{11}	0.94 ± 0.002 (0.94 ± 0.001)
m_{12}	1.0 ± 0.002 (1.0 ± 0.002)
m_{13}	−0.38 ± 0.003 (−0.51 ± 0.002)

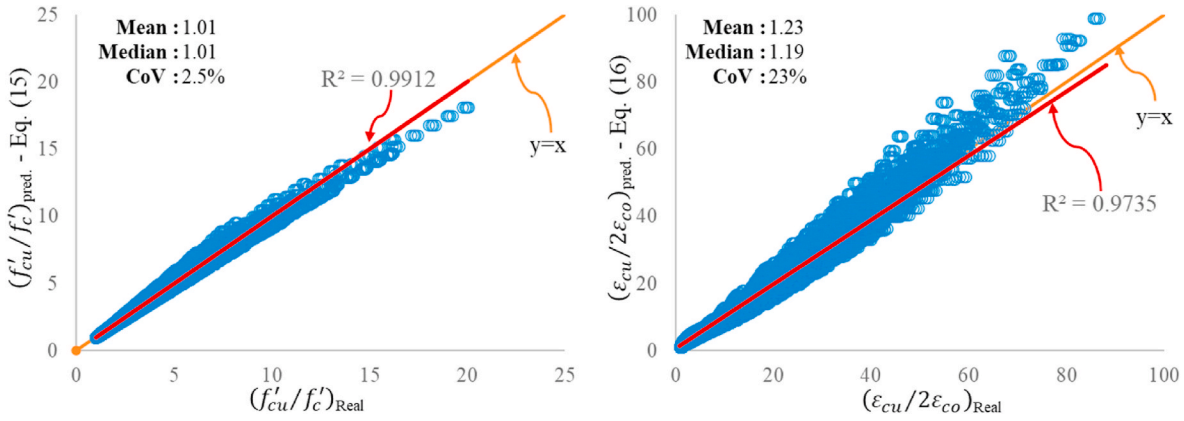

Fig. 20. The comparison real and predicted values analytically generated RC sections.

coefficient, mean, median and coefficient of variation (CoV) values for the ratios prediction to real values were also computed and given in the Figure. Based on the obtained values, it can be said that mean and median values are comparable and the variation between real and proposed values are low which highlights the efficiency of proposed equations. Accordingly, it can be implied that proposed prediction equations have very good accuracy in predicting the stress and strain values for FRP-confined concrete at ultimate conditions.

Following the analytical comparisons, proposed model is then compared with experimental results based on both stress-strain [18,19,22,41–46] and moment-curvature relation of FRP-confined sections [38,47,48]. To avoid excessive use of figures, some of stress-strain relationship using existing models are compared with proposed model in Fig. 21. In the figure, notations of "S" and "R" at the beginning of experimental model name are used to describe the square and rectangular sections, respectively. The comparison of rest of experimental results with proposed model is made in Table 5 to make comprehensive assessment and to illustrate efficiency of proposed models using some statistical parameters such as mean, median, root mean squared error (RMSE), mean absolute error (MAE) and average absolute error (AAE). The brief information regarding physical properties of member sections in experimental specimens are presented in Appendix A.

It can be seen from Fig. 21 that existing models may produce different stress-strain relations compared to each other. Nevertheless, stress-strain relation of proposed and Lam and Teng model is similar. Proposed model assumes the linear relation between initial and f'_c and ε_{co} (accepted as equal to 0.002) points, this assumption may cause slightly underestimation of initial stiffness. On the other hand, the figure also demonstrates that some existing models depending on the experiment might also underestimate the initial stiffness for the stress-strain relation despite the extensive calculations. It should be noted that both stress-strain values of experiments at yield and ultimate is comparable to proposed model. The absolute error (experiment-predicted) of stress and strain at ultimate presented in Fig. 21 is less than %7 and %9, respectively. Considering the experiment presented in Fig. 21 and some published experimental results are computed and compared with proposed model in Table 5. It is wort noting that experimental specimens represent broad range of specimens. For example, specimens cover different section dimensions (i.e., square and rectangular), compressive concrete strength (f'_c), corner radius (r_c) and wide range of FRP material characteristics (f_{ju}, k_ε and t_j) as can be seen in Appendix A. By this way, comprehensive assessment was made through proposed and existing predictive models and results are given in Table 5. In the table, specimens and experimental results are introduced in first three rows and later stress and strain values produced by proposed, Ilki, Lam and Teng (LT), Pantelides and Youssef models are given. In the last five rows of the table, some statistical parameters are used to investigate efficiency of proposed model by comparing the existing models.

According to Table 5, proposed model in the 3rd rank for prediction of stress at ultimate according to mean of experiment/model

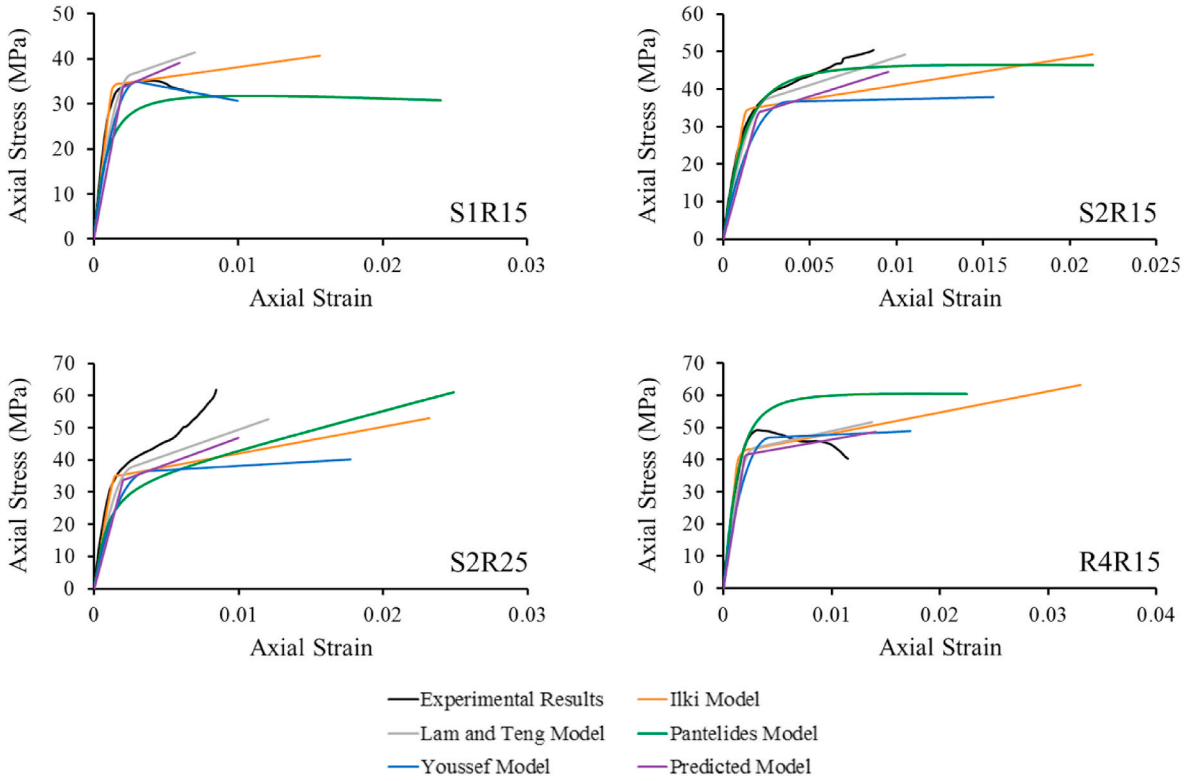

Fig. 21. The comparison stress-strain relation of proposed model with existing and experimental results.

results of 1.09, 0.95, 1.03, 0.97 and 1.22 for proposed, Ilki, Lam and Teng (LT), Pantelides and Youssef models, respectively. This situation is also valid for mean of absolute of values 1-(Experiment/model)**.** On the other hand, when the ultimate stress values are compared for the same statistical parameters, proposed model in the 2nd rank after Lam and Teng model and it should be noted that calculated values for Lam and Teng models are very close to proposed model. Although the ranking between the models varies depending on the statistical parameter (i.e., mean of absolute of values 1-(Experiment/model)**,** (Experiment/model) and Median), it can be said that the proposed model and Lam and Teng results are the most compatible with experimental results. Similar conclusions can be also drawn for strain results of models and proposed one.

When the results for statistical parameters of AAE, RMSE and MAE are compared over the stress values produced, it can be observed that Lam and Teng and proposed model results are identical for AAE and calculated RMSE and MAE values for Lam and Teng model are found slightly lower than proposed model. For example, RMSE and MAE values of proposed and Lam and Teng values are 9.12 and 6.92, and 8.28 and 6.66, respectively. However, when the comparisons are also made over the strain predictions for RMSE and MAE, it can be apparently seen that the proposed model (RMSE = 0.0026 and MAE = 0.0020) is in the first rank compared to existing models.

The comparison of proposed model with existing models also extended for moment-curvature response of experimental results. As mentioned in previous sections, moment-curvature response of FRP-confined members are not evaluated in detail. For this reason, the number of experimental results on the moment-curvature responses are limited [38,47,48] and available literature used for assessment purposes. Experimental results of Iacobucci [38] were given in Section 3 and comparison of existing models were made (see Fig. 6) in the related section. For this reason, moment-curvature response of all models is not provided in this section and only experimental results are plotted for proposed and Lam and Teng models which was found the best two ranked models earlier. However, statistical assessment for existing models including proposed model is made in Table 6. The experimental results of Sause et al. [47] and Walkup [48] were used for comparison and the label of these experiments were F1 and F2. Information regarding F1 and F2 specimens are also given in Appendix A. F1 and F2 specimens have equal dimension in both directions (i.e., square) and these specimens were subjected to cyclic tests. Cyclic response of columns was determined under constant axial load (1339 kN and 1352 kN for F1 and F2, respectively) and results are plotted in Fig. 22. In the figure, designation of reinforcing steel and section dimensions for specimens are also sketched. It can be seen from the figure that moment-curvature capacity of columns determined from proposed model is remarkably close to responses determined from Lam and Teng model. Figure also indicates that that initial stiffness of moment-curvature determined from proposed model is also in agreement with experimental results. According to comparisons, it can be said that proposed model and Lam and Teng model slightly underestimates the ultimate curvature capacity of sections. However, it is worth noting that curvature capacities of specimens at ultimate are slightly higher since these values calculated by averaging the maximum curvatures from positive and negative cycles.

The moment and curvature responses experiments and existing models including proposed one are tabulated in Table 6 and

Table 5
The comparison of proposed model with existing models using experimental results at ultimate condition (units in MPa for compressive strength).

Specimen	f'_{cu} (Exp.)	ε_{cu} (Exp.)	f'_{cu} (Eq. (15))	ε_{cu} (Eq. (16).)	f'_{cu} (Ilki)	ε_{cu} (Ilki)	f'_{cu} (LT)	ε_{cu} (LT)	f'_{cu} (Pant.)	ε_{cu} (Pant.)	f'_{cu} (Yous.)	ε_{cu} (Yous.)
S–C2-0 [18]	26.1	0.01	21.86	0.009	27.12	0.026	26.19	0.013	26.11	0.01	20.11	0.02
S1R15 [19]	35	0.007	39.14	0.006	40.74	0.016	41.44	0.007	31.79	0.024	34.93	0.01
S1R25 [19]	39.4	0.009	40.27	0.006	42.39	0.017	43.17	0.008	38.35	0.026	34.87	0.011
S2R15 [19]	50.4	0.009	44.58	0.010	49.26	0.021	49.19	0.01	46.45	0.021	37.83	0.016
S2R25 [19]	61.9	0.008	46.84	0.010	52.98	0.023	52.64	0.012	61.05	0.025	40.15	0.018
S3R15 [19]	61.6	0.018	40.32	0.014	50.3	0.030	47.23	0.018	54.14	0.017	35.37	0.028
S3R25 [19]	66	0.015	43.72	0.016	56.66	0.033	52.4	0.021	69.44	0.02	37.95	0.033
R4R15 [19]	49.2	0.012	48.64	0.014	63.18	0.033	51.62	0.014	60.44	0.022	48.83	0.017
R4R25 [19]	51.9	0.01	50.12	0.015	68.95	0.036	53.72	0.016	78.49	0.026	52.27	0.02
R3b [22]	38.4	0.013	36.71	0.011	46.55	0.038	37.62	0.012	52.49	0.024	36.82	0.013
S5–C5 [41]	43.9	0.01	52.83	0.010	57.62	0.018	58.16	0.008	41.37	0.018	48.42	0.012
S25–C4 [41]	50.9	0.014	56.86	0.011	62.4	0.021	62.82	0.01	66.25	0.025	47.85	0.014
R25-C3 [41]	42	0.008	46.37	0.009	52.03	0.022	48.37	0.008	44.64	0.024	43.89	0.01
R38-C3 [41]	43.7	0.009	47.1	0.010	54.04	0.023	49.57	0.009	56.96	0.028	43.81	0.011
R5-C5 [41]	44.3	0.01	47.91	0.012	54.13	0.021	50.51	0.008	41.06	0.021	47.69	0.01
R25-C4 [41]	44.3	0.009	49.72	0.010	57.79	0.024	52.4	0.009	54.52	0.024	46.61	0.012
R2-30 [42]	32	0.008	33.77	0.008	37.1	0.021	34.84	0.008	29.21	0.018	31.29	0.011
ScL5m [43]	55.6	0.011	48.43	0.012	53.57	0.024	52.89	0.012	60.64	0.021	40.4	0.018
s-r50 [44]	61.7	0.011	46.82	0.012	44.94	0.025	45.58	0.013	70.1	0.021	33.52	0.017
s-r50 [44]	63.7	0.011	48.36	0.012	46.32	0.024	47.12	0.012	71.6	0.022	34.75	0.017
R4Lr45 [45]	45.2	0.025	38.81	0.019	54.68	0.041	39.89	0.019	62.91	0.019	40.04	0.024
R2Lr25 [45]	42.1	0.014	39.19	0.009	43.73	0.024	39.66	0.009	33.06	0.02	37.54	0.011
R4Lr65 [45]	51.1	0.026	40.26	0.021	59.66	0.044	41.65	0.021	77.14	0.021	42.35	0.027
P-1-20-3-A [46]	27.3	0.008	30.07	0.007	30.5	0.018	30.84	0.008	23.2	0.017	25.05	0.012
P-1.5-40-2-A [46]	28.7	0.008	24.25	0.006	27.04	0.024	24.63	0.008	22.3	0.02	22.92	0.011
P-1.5-20-2-A [46]	29.3	0.007	25.24	0.005	27.19	0.02	25.56	0.007	21.96	0.023	24.44	0.009
(Experiment/model) $_{mean}$			1.09	1.07	0.95	0.45	1.03	1.02	0.97	0.57	1.22	0.76
|1-(Experiment/model)| $_{mean}$			0.16	0.18	0.16	0.55	0.14	0.17	0.16	0.48	0.24	0.27
Median (Experiment/model)			1.06	0.98	0.88	0.44	1.01	0.99	0.98	0.49	1.13	0.75
AAE			0.14	0.17	0.17	1.33	0.14	0.17	0.18	1.13	0.16	0.43
RMSE			9.12	0.0026	9.79	0.0217	8.28	0.0050	10.77	0.0192	12.81	0.0069
MAE			6.92	0.0020	8.32	0.0141	6.66	0.0021	8.23	0.0107	8.51	0.0046

Table 6
The comparison of moment and curvature responses determined from proposed and existing models using experimental results at ultimate condition.

Specimen	M_u (kNm) (Exp.)	φ_u (1/m) (Exp.)	M_u (kNm) (Prop.)	φ_u (1/m) (Prop.)	M_u (kNm) (Ilki)	φ_u (1/m) (Ilki)	M_u (kNm) (LT)	φ_u (1/m) (LT)	M_u (kNm) (Pant.)	φ_u (1/m) (Pant.)	M_u (kNm) (Yous.)	φ_u (1/m) (Yous.)
ASC-2NS	228.8	0.126	227.91	0.088	229.99	0.088	231.82	0.089	226.45	0.209	220.49	0.083
ASC-3NS	233.2	0.120	237.67	0.066	244.42	0.086	246.91	0.068	227.77	0.105	227.12	0.063
ASC-4NS	218.2	0.065	231.70	0.065	233.50	0.065	236.35	0.066	227.95	0.166	218.47	0.059
ASC-5NS	260.1	0.150	245.20	0.066	255.39	0.107	257.17	0.070	228.89	0.081	235.91	0.065
ASC-6NS	245.8	0.163	233.92	0.088	240.10	0.111	240.65	0.091	227.80	0.137	225.58	0.085
F1	529.8	0.117	495.50	0.079	512.60	0.160	500.80	0.086	519.30	0.128	482.62	0.101
F2	500.1	0.107	493.28	0.075	504.55	0.126	498.58	0.081	491.26	0.112	475.68	0.071
AAE			0.04	0.34	0.03	0.27	0.04	0.32	0.04	0.44	0.05	0.35
RMSE			15.98	0.05	10.21	0.04	14.16	0.05	15.20	0.06	23.66	0.05
MAE			12.39	0.04	8.53	0.03	10.50	0.04	12.30	0.04	18.66	0.05

assessed by some of statistical parameters. Due to limited number of experiments, mean and median values are not calculated in the table and AEE, RMSE and MAE parameters are used. According to Table 6, AEE values determined from all models are very close for moment responses at ultimate, the maximum and minimum AEE value are 0.03 (determined for Ilki model) and 0.05 (determined for Youssef model), respectively. AEE is equal to 0.04 for rest models including proposed model. According to Table 6, proposed model in the 2nd rank with Lam and Teng model for the prediction of moment capacity at ultimate according to AEE. This situation is also valid when the ultimate curvature capacities are compared for the same statistical parameter (i.e. AEE). It seems that Ilki model produced more compatible results compared to experiments. Similar conclusions can be also drawn for strain results of models and proposed one. This is partly related to constitutive model of Ilki model since stress and strain values of relatively higher than all compared existing models. In addition, averaging of maximum curvatures from positive and negative cycles from experiments at ultimate were found slightly higher than individual cycles. Accordingly, similarity of Ilki model with experiments was expected.

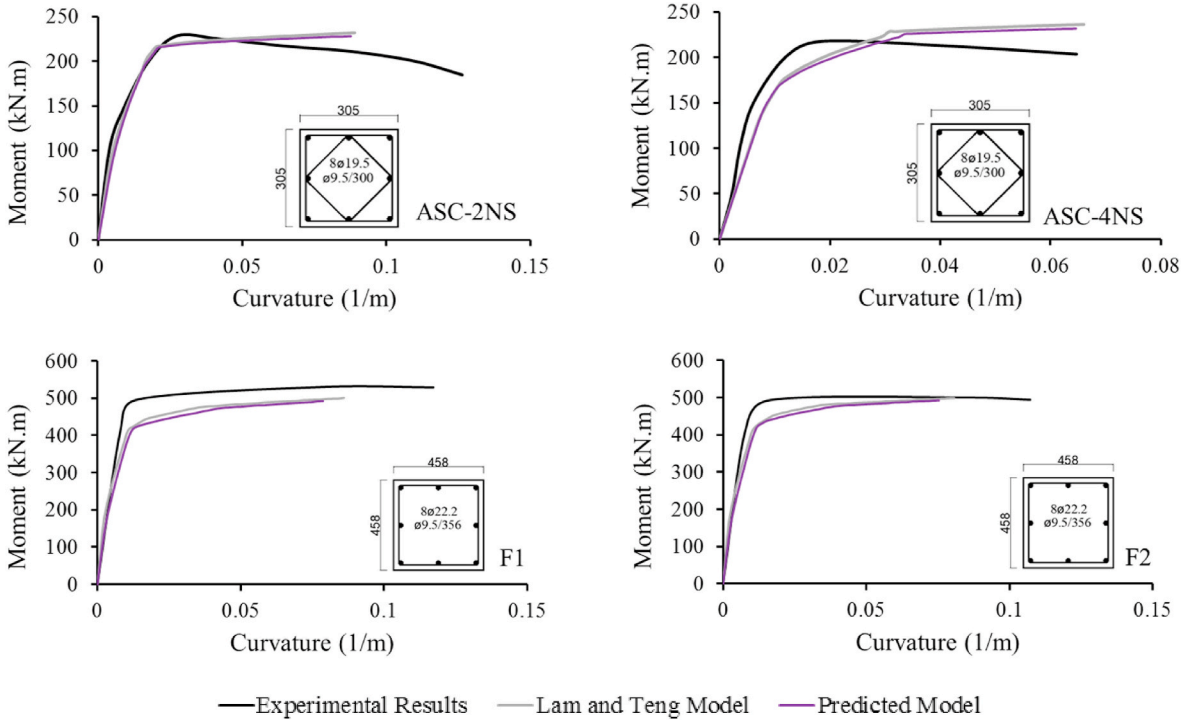

Fig. 22. The comparison moment-curvature behavior of proposed model with Lam and Teng and experimental results.

When the results for statistical parameters of RMSE and MAE are compared over the moment capacities, Ilki model found close to experimental values and Lam and Teng and proposed model can be place in 2nd and 3rd rank, respectively. Calculated RMSE and MAE values over curvature capacities indicate that Lam and Teng and proposed model results are close. For example, RMSE values are identical and equal to 0.05, and MAE values are 0.04 and 0.05 for proposed model and Lam and Teng model, respectively. Considering the MAE value, proposed model is in the second rank among the existing models. Consequently, when the results of analytical and experiments for both stress-strain and moment-curvature relations considered, proposed model can be found accurate and comparable to existing models with low error and variation. Proposed model can be also regarded as efficient since proposed equation significantly practical and reduces time and computational efforts compared to existing FRP-confined models.

6. Conclusion

In this study, effects of FRP-confined models on the stress, strain, N-M relation and moment and curvature capacity were examined by using numerous as-built RC section database. Based on the statistical analyses, simple prediction equations were proposed for the estimation of stress and strain based on bi-linear approximation. Based on the comparisons, following conclusions and recommendations made as follows.

- Analysis results have shown that depending on the model, concrete strength gain may up to 2.5 times compared to unconfined concrete. Similar gain ratios were also obtained for curvature at ultimate. On the other hand, the effect of FRP confining on the strain is more pronounced than strength capacity and strain gain may be 4 times higher than unconfined concrete.
- Comparison N-M interaction of FRP-confined models showed that FRP confining have positive impact on the moment capacity of sections compared to ordinary confined concrete model. It was also observed that the effect of FRP becomes more apparent especially if the reinforcement ratio increases when axial loads around the zero.
- Based on the extensive statistical evaluations on the FRP-confined concrete using numerous generated RC sections, it was determined that ultimate stress and strain capacity of FRP-confined model can be described as function of $h/b, r_c, f'_c, f_{ju}, k_\varepsilon$ and ρ_j parameters. Statistical analyses have shown that strength and strain value at ultimate can be identified as linear and power functions, respectively. Finally, constitutive model for design-oriented FRP-confined model based bi-linear backbone curve is proposed.
- Proposed model including existing models was subjected to a comparison with analytical and experimental results and accuracy of model was investigated. Comparison of proposed with analytically generated RC sections showed that the correlation coefficient was higher than 0.97 for both stress and strain predictions. In addition, statistical measures of mean, median and coefficient of variations were found 1.01, 1.01, 2.5 % and 1.23, 1.19, 23 % for stress and strain, respectively. Considering the high correlations and low variations, proposed equations was found accurate in predicting the stress and strain values for FRP-confined concrete at ultimate conditions.

- Comparison of proposed model with experimental results at ultimate was also made existing FRP-confined model and results evaluated in terms of different statistical measures. According to quantitative assessment, mean of experiment/model, median, average absolute error (AAE), root mean squared error (RMSE), mean absolute error (MAE) parameters were found 1.09, 1.06, 0.14, 9.12 and 6.92 for stress and 1.07, 0.98, 0.17, 0.0026 and 0.0020 for strain, respectively. When both stress and strain values are evaluated together, proposed model provided good accuracy considering the statistical measures compared to existing models.
- Moment and curvature response of FRP-confined members are also evaluated. According to results, AAE, RMSE and MAE parameters were found 0.04, 15.98 and 12.39 for moment capacity and 0.34, 0.05 and 0.04 for curvature, respectively. Comparison of calculated statistical measures indicated proposed models are very close and comparable to the other models of Ilki and Lam and Teng models.
- Based on the results of both analytical and experiments for both stress-strain and moment-curvature relations, proposed model with low error and variation, found accurate and comparable to existing models. Furthermore, proposed model can be assumed as efficient considering the practicality of proposed model which reduces time and computational efforts.

Funding

No funding was received.

CRediT authorship contribution statement

Mehmet Palanci: Writing – original draft, Visualization, Validation, Supervision, Methodology. **Ilker Subasi:** Writing – original draft, Validation, Investigation, Data curation.

Declaration of competing interest

The authors declare that they have no known competing financial interests or personal relationships that could have appeared to influence the work reported in this article.

Data availability

Data will be made available on request.

Appendix A. The information regarding experiments used in this study for the comparison and validation

Specimen	b (mm)	h (mm)	h/b	$f_c^{'}$ (MPa)	r_c (mm)	$f_{ju}^{'}$ (MPa)	t_j (mm)	k_e
S–C2-0 [18]	279	279	1.00	15.20	19	1120	2	0.59
S1R15 [19]	150	150	1.00	33.70	15	4519	0.17	0.59
S1R25 [19]	150	150	1.00	33.70	25	4519	0.17	0.59
S2R15 [19]	150	150	1.00	33.70	15	4519	0.33	0.59
S2R25 [19]	150	150	1.00	33.70	25	4519	0.33	0.59
S3R15 [19]	150	150	1.00	24.00	15	4519	0.5	0.59
S3R25 [19]	150	150	1.00	24.00	25	4519	0.5	0.59
R4R15 [19]	150	225	1.50	41.50	15	4519	0.66	0.59
R4R25 [19]	150	225	1.50	41.50	25	4519	0.66	0.59
R3b [22]	150	300	2.00	34.00	40	3430	0.5	0.59
S5–C5 [41]	152	152	1.00	43.90	5	1265	1.5	0.58
S25–C4 [41]	152	152	1.00	43.90	25	1265	1.2	0.58
R25-C3 [41]	152	203	1.34	42.00	25	1265	0.9	0.58
R38-C3 [41]	152	203	1.34	42.00	38	1265	0.9	0.58
R5-C5 [41]	152	203	1.34	43.90	5	1265	1.5	0.58
R25-C4 [41]	152	203	1.34	43.90	25	1265	1.2	0.58
R2-30 [42]	94	118	1.26	29.50	10	3550	0.17	0.8
ScL5m [43]	200	200	1.00	33.04	30	3720	0.59	0.59
s-r50 [44]	150	150	1.00	26.72	50	939	1.2	0.92
s-r50 [44]	150	150	1.00	28.26	50	939	1.2	0.92
R4Lr45 [45]	290	435	1.50	28.90	45	3993	1.34	0.59
R2Lr25 [45]	290	435	1.50	35.20	25	3993	0.67	0.59
R4Lr65 [45]	290	435	1.50	28.90	65	3993	1.34	0.59
P-1-20-3-A [46]	300	300	1.00	23.54	20	4161	0.39	0.59
P-1.5-40-2-A [46]	250	375	1.50	22.03	40	4161	0.26	0.59
P-1.5-20-2-A [46]	250	375	1.50	23.53	20	4161	0.26	0.59
F1 [47,48]	458	458	1.00	22.70	45	580	6	0.58*
F2 [47,48]	458	458	1.00	24.80	45	580	4	0.58*

* Assumed during analysis.

References

[1] S.Z. Korkmaz, Observations on the van earthquake and structural failures, J. Perform. Constr. Facil. 29 (2015), https://doi.org/10.1061/(asce)cf.1943-5509.0000456.
[2] O. Onat, B. Yön, M.E. Öncü, S. Varolgüneş, A. Karaşin, S. Cemalgil, Field reconnaissance and structural assessment of the October 30, 2020, Samos, Aegean Sea earthquake: an example of severe damage due to the basin effect, Nat. Hazards 112 (2022) 75–117, https://doi.org/10.1007/s11069-021-05173-y.
[3] B. Yon, E. Sayın, T.S. Koksal, Seismic response of buildings during the May 19, 2011 Simav, Turkey earthquake, Earthquakes Struct 5 (2013) 343–357, https://doi.org/10.12989/eas.2013.5.3.343.
[4] A.C. Altunişik, M.E. Arslan, V. Kahya, B. Aslan, T. Sezdirmez, G. Dok, O. Kirtel, H. Öztürk, F. Sunca, A. Baltaci, M. Emiroğlu, M. Günaydin, S. Adanur, B. Atmaca, T. Akgül, A. Demir, T. Tatar, B. Aykanat, K. Haciefendioğlu, A. Saribiyik, M. Yurdakul, Y.E. Akbulut, F.Y. Okur, F. Şen, A.F. Genç, H.B. Başağa, E. Demirkaya, O. Güleş, M. Nas, Field observations and damage evaluation in reinforced concrete buildings after the february 6th, 2023, kahramanmaraş–türkiye earthquakes, J. Earthq. Tsunami 17 (2023), https://doi.org/10.1142/S1793431123500240.
[5] N. Caglar, I. Vural, O. Kirtel, A. Saribiyik, Y. Sumer, Structural damages observed in buildings after the January 24, 2020 Elazığ-Sivrice earthquake in Türkiye, Case Stud. Constr. Mater. 18 (2023) e01886, https://doi.org/10.1016/j.cscm.2023.e01886.
[6] C. Cirak Karakas, M. Palanci, S.M. Senel, Fragility based evaluation of different code based assessment approaches for the performance estimation of existing buildings, Bull. Earthq. Eng. 20 (2022) 1685–1716, https://doi.org/10.1007/s10518-021-01292-w.
[7] M. Palanci, A. Kalkan, S.M. Senel, Investigation of shear effects on the capacity and demand estimation of RC buildings, Struct. Eng. Mech. 60 (2016) 1021–1038, https://doi.org/10.12989/sem.2016.60.6.1021.
[8] M. Palanci, A.H. Kayhan, A. Demir, A statistical assessment on global drift ratio demands of mid-rise RC buildings using code-compatible real ground motion records, Bull. Earthq. Eng. 16 (2018) 5453–5488, https://doi.org/10.1007/s10518-018-0384-y.
[9] T. Ozbakkaloglu, J.C. Lim, T. Vincent, FRP-confined concrete in circular sections: review and assessment of stress-strain models, Eng. Struct. 49 (2013) 1068–1088, https://doi.org/10.1016/j.engstruct.2012.06.010.
[10] K.G. Vandoros, S.E. Dritsos, Concrete jacket construction detail effectiveness when strengthening RC columns, Constr. Build. Mater. 22 (2008) 264–276, https://doi.org/10.1016/j.conbuildmat.2006.08.019.
[11] T.M. Pham, M.N.S. Hadi, Stress prediction model for FRP confined rectangular concrete columns with rounded corners, J. Compos. Constr. 18 (2014), https://doi.org/10.1061/(ASCE)CC.1943-5614.0000407.
[12] A. Hosseini, A.R. Khaloo, S. Fadaee, Seismic performance of high-strength concrete square columns confined with carbon fiber reinforced polymers (CFRPs), Can. J. Civ. Eng. 32 (2005) 569–578, https://doi.org/10.1139/l05-006.
[13] M.H. Harajli, Axial stress-strain relationship for FRP confined circular and rectangular concrete columns, Cem. Concr. Compos. 28 (2006) 938–948, https://doi.org/10.1016/j.cemconcomp.2006.07.005.
[14] M.H. Harajli, E. Hantouche, K. Soudki, Stress-strain model for fiber-reinforced polymer jacketed concrete columns, ACI Struct. J. 103 (2006) 672–682, https://doi.org/10.14359/16919.
[15] M.N. Youssef, M.Q. Feng, A.S. Mosallam, Stress-strain model for concrete confined by FRP composites, Compos. Part B Eng. 38 (2007) 614–628, https://doi.org/10.1016/j.compositesb.2006.07.020.
[16] Y.Y. Wei, Y.F. Wu, Unified stress-strain model of concrete for FRP-confined columns, Constr. Build. Mater. 26 (2012) 381–392, https://doi.org/10.1016/j.conbuildmat.2011.06.037.
[17] C.P. Pantelides, Z. Yan, L.D. Reaveley, Shape modification of rectangular columns confined with FRP composites, Rep. No. UT-05.03 (2004) 1–179. https://trid.trb.org/view/1243702. (Accessed 9 October 2022).
[18] C.P. Pantelides, Z. Yan, Confinement model of concrete with externally bonded FRP jackets or posttensioned FRP shells, J. Struct. Eng. 133 (2007) 1288–1296.
[19] L. Lam, J.G. Teng, Design-oriented stress–strain model for FRP-confined concrete, Constr. Build. Mater. 17 (2003) 471–489, https://doi.org/10.1016/S0950-0618(03)00045-X.
[20] L. Lam, J.G. Teng, Design-oriented stress-strain model for FRP-confined concrete in rectangular columns, J. Reinf. Plast. Compos. 22 (2003) 1149–1186, https://doi.org/10.1177/0731684403035429.
[21] A. Ilki, N. Kumbasar, V. Koc, Low strength concrete members externally confined with FRP sheets, Struct. Eng. Mech. 18 (2004) 167–194, https://doi.org/10.12989/sem.2004.18.2.167.
[22] A. Ilki, N. Kumbasar, Compressive behaviour of carbon fibre composite jacketed concrete with circular and non-circular cross-sections, J. Earthq. Eng. 7 (2003) 381–406, https://doi.org/10.1080/13632460309350455.
[23] G. Lin, Seismic Performance of FRP-Confined RC Columns: Stress-Strain Models and Numerical Simulation, The Hong Kong Polytechnic University, 2016. https://theses.lib.polyu.edu.hk/handle/200/8695.
[24] J.C. Lim, M. Karakus, T. Ozbakkaloglu, Evaluation of ultimate conditions of FRP-confined concrete columns using genetic programming, Comput. Struct. 162 (2016) 28–37, https://doi.org/10.1016/j.compstruc.2015.09.005.
[25] H. Naderpour, A. Kheyroddin, G.G. Amiri, Prediction of FRP-confined compressive strength of concrete using artificial neural networks, Compos. Struct. 92 (2010) 2817–2829, https://doi.org/10.1016/j.compstruct.2010.04.008.
[26] K. Jiang, Q. Han, Y. Bai, X. Du, Data-driven ultimate conditions prediction and stress-strain model for FRP-confined concrete, Compos. Struct. 242 (2020) 112094, https://doi.org/10.1016/j.compstruct.2020.112094.
[27] Y. Wu, G. Jin, T. Ding, D. Meng, Modeling confinement efficiency of FRP-confined concrete column using radial basis function neural network, in: 2010 2nd Int. Work. Intell. Syst. Appl., IEEE, 2010, pp. 1–6, https://doi.org/10.1109/IWISA.2010.5473464.
[28] A. Cascardi, F. Micelli, M.A. Aiello, An Artificial Neural Networks model for the prediction of the compressive strength of FRP-confined concrete circular columns, Eng. Struct. 140 (2017) 199–208, https://doi.org/10.1016/j.engstruct.2017.02.047.
[29] T.M. Pham, M.N.S. Hadi, Predicting stress and strain of FRP-confined square/rectangular columns using artificial neural networks, J. Compos. Constr. 18 (2014), https://doi.org/10.1061/(ASCE)CC.1943-5614.0000477.
[30] A. Fallah Pour, A. Gholampour, An artificial network-based prediction of key reference zones on axial stress–strain curves of FRP-confined concrete, Appl. Sci. 13 (2023) 3038, https://doi.org/10.3390/app13053038.
[31] ACI 440, Guide for the Design and Construction of Externally Bonded FRP Systems for Strengthening Concrete Structures, ACI 440.2R, American Concrete Institute, 2008.
[32] G. Yavuz, Lif takviyeli polimerlerin betonarme kirişlerde donatı olarak kullanımı, E-journal new world sci. Acad, Eng. Sci. 6 (2011) 1001–1015. http://ridum.umanizales.edu.co:8080/jspui/bitstream/6789/377/4/Muñoz_Zapata_Adriana_Patricia_Artículo_2011.pdf.
[33] J.B. Mander, M.J.N. Priestley, R. Park, Theoretical stress-strain model for confined concrete, J. Struct. Eng. 114 (1988) 1804–1826.
[34] M. Palanci, Flexural response prediction of reinforced concrete members based on statistical observations, Arab. J. Sci. Eng. 42 (2017) 3689–3709, https://doi.org/10.1007/s13369-016-2392-z.
[35] E. Hognestad, A study of combined bending and axial load in reinforced concrete members, ideals.illinois.edu/handle/2142/4360%0A, Bull. Ser. No. 399 (1951) 128. hdl.handle.net/2142/4360.
[36] R.M. Richard, B.J. Abbott, Versatile elastic-plastic stress-strain formula, J. Eng. Mech. Div. 101 (1975) 511–515, https://doi.org/10.1061/jmcea3.0002047.
[37] TBEC, Turkish Building Earthquake Code, Disaster and Emergency Management Presidency, Ankara, Turkiye, 2018.
[38] R.D. Iacobucci, S.A. Sheikh, O. Bayrak, Retrofit of square concrete columns with carbon fiber-reinforced polymer for seismic resistance, ACI Struct. J. 100 (2003) 785–794.
[39] S. Rocca, N. Galati, A. Nanni, Interaction diagram methodology for design of FRP-confined reinforced concrete columns, Constr. Build. Mater. 23 (2009) 1508–1520, https://doi.org/10.1016/j.conbuildmat.2008.06.010.

[40] C. Pellegrino, C. Modena, Analytical model for FRP confinement of concrete columns with and without internal steel reinforcement, J. Compos. Constr. 14 (2010) 693–705, https://doi.org/10.1061/(ASCE)CC.1943-5614.0000127.
[41] P. Rochette, P. Labossière, Axial testing of rectangular column models confined with composites, J. Compos. Constr. 4 (2000) 129–136.
[42] I.A.E.M. Shehata, L.A.V. Carneiro, L.C.D. Shehata, Strength of short concrete columns confined with CFRP sheets, Mater. Struct. 35 (2002) 50–58, https://doi.org/10.1007/BF02482090.
[43] T.C. Rousakis, A.I. Karabinis, P.D. Kiousis, FRP-confined concrete members: axial compression experiments and plasticity modelling, Eng. Struct. 29 (2007) 1343–1353, https://doi.org/10.1016/j.engstruct.2006.08.006.
[44] Y.A. Al-Salloum, Influence of edge sharpness on the strength of square concrete columns confined with FRP composite laminates, Compos. Part B Eng. 38 (2007) 640–650, https://doi.org/10.1016/j.compositesb.2006.06.019.
[45] J.J. Zeng, G. Lin, J.G. Teng, L.J. Li, Behavior of large-scale FRP-confined rectangular RC columns under axial compression, Eng. Struct. 174 (2018) 629–645, https://doi.org/10.1016/j.engstruct.2018.07.086.
[46] V.J. Castro, F.J. León, S. Martínez, A. de Diego, L. Echevarría, Effectiveness of CFRP jackets in RC rectangular columns. Full-scale experimental study, Constr. Build. Mater. 416 (2024) 134840, https://doi.org/10.1016/j.conbuildmat.2023.134840.
[47] R. Sause, K.A. Harries, S.L. Walkup, S. Pessiki, J.M. Ricles, Flexural behavior of concrete columns retrofitted with carbon fiber-reinforced polymer jackets, ACI Struct. J. 101 (2004), https://doi.org/10.14359/13393.
[48] S.L. Walkup, Rehabilitation of Non-ductile Reinforced Concrete Building Columns Using Fiber Reinforced Polymer Jackets, Lehigh University, 1998.